END
DATE
FILMED
12-77
DDC

"ON THE JAHN-TELLER EFFECT IN IrF$_6$:   THE

Γ_{8g} $(t_{2g})^3$ STATE AT 6800 Å"

by

E. R. Bernstein and J. D. Webb

Department of Chemistry
Colorado State University
Fort Collins, Colorado 80523

October 1977

AD-*A046 563* Date *29 Nov 77*

To: DDC-TA

Title to be verbalized by DDC-TA.

☑ Field 6

☐ Field 7

Olga G. Luchaka
DDC-TCD

(Note to be removed <u>after</u> <u>Proofreading</u>
TST-1).

Gamma sub 8g
— thrice degenerate. t sub 2g

REPORT DOCUMENTATION PAGE		READ INSTRUCTIONS BEFORE COMPLETING FORM
1. REPORT NUMBER (14) TR - 15	2. GOVT ACCESSION NO.	3. RECIPIENT'S CATALOG NUMBER
4. TITLE (and Subtitle) On the Jahn-Teller Effect in IrF$_6$: The $\Gamma_{8g}(t_{2g})^3$ State at 6800 Å.		5. TYPE OF REPORT & PERIOD COVERED Technical Report.
		6. PERFORMING ORG. REPORT NUMBER
7. AUTHOR(s) E. R. Bernstein and J. D. Webb		8. CONTRACT OR GRANT NUMBER(s) N00014-75-C-1179
9. PERFORMING ORGANIZATION NAME AND ADDRESS Department of Chemistry, Colorado State University Fort Collins, CO 80523		10. PROGRAM ELEMENT, PROJECT, TASK AREA & WORK UNIT NUMBERS NR 056-607
11. CONTROLLING OFFICE NAME AND ADDRESS Office of Naval Research Arlington, VA 22217		12. REPORT DATE October 1977
		13. NUMBER OF PAGES 61
14. MONITORING AGENCY NAME & ADDRESS(if different from Controlling Office) 59p.		15. SECURITY CLASS. (of this report) Unclassified
		15a. DECLASSIFICATION/DOWNGRADING SCHEDULE

16. DISTRIBUTION STATEMENT (of this Report)

Approved for Public Release; Distribution Unlimited.

17. DISTRIBUTION STATEMENT (of the abstract entered in Block 20, if different from Report)

18. SUPPLEMENTARY NOTES

19. KEY WORDS (Continue on reverse side if necessary and identify by block number)

vibronic coupling
IrF$_6$
Jahn-Teller effect
crystal field splitting
second order vibronic coupling

general vibronic coupling
excited state IrF$_6$ vibrations

Gamma sub 8g   *from — Gamma sub 7g*   *Gamma sub 8g*

20. ABSTRACT (Continue on reverse side if necessary and identify by block number)

In this work we present a detailed discussion of the highest energy d-d transitions of IrF$_6$, $\Gamma_{8g}(^2T_{2g}) \leftarrow \Gamma_{8g}(^4A_{2g})$ at 14,900 cm^{-1} and $\Gamma_{7g}(^2T_{2g}) \leftarrow \Gamma_{8g}(^4A_{2g})$ at 12,100 cm^{-1}, as observed in dilute mixed crystals with UF$_6$, MoF$_6$, and WF$_6$ at 4.2 and 1.8 K. The system is of particular interest because Γ_{8g} —$\rightarrow$ next pg

Gamma sub 8g   *sub 2g*

DD FORM 1473 1 JAN 73   EDITION OF 1 NOV 65 IS OBSOLETE
S/N 0102-014-6601

404992

20.

states are Jahn-Teller active and the Γ_{7g} state serves as an excellent example of what may be expected for a similar but non-Jahn-Teller active state. It is found that the usual linear Jahn-Teller interaction involving either $\nu_2(e_g)$ or $\nu_5(t_{2g})$ cannot account for the observations of both shifts and splittings of $\nu_5(\Gamma_{8g})$. In order to explain all the relevant observations, theories encompassing higher order vibronic coupling terms and/or coupled ν_2-ν_5 linear effects must be considered. Based on calculations, IrF_6^{n} is assigned an approximate D_{4h} symmetry in the mixed crystals. A new electronic charge transfer state (Γ_{7g} or Γ_{6g}) is located at ~15,900/cm and stretching vibration n (ν_1', ν_2', ν_3') (n = 1, 2) are identified built on this origin.

ACCESSION for

NTIS

DDC

UNANNOUNCED

JUSTIFICATION

BY

DISTRIBUTION/AVAILABILITY CODES

Dist.

I.   INTRODUCTION

The breakdown of the Born-Oppenheimer approximation in the special case of two- and three-fold orbitally degenerate electronic states (the Jahn-Teller effect[1]) has received a great deal of recent attention.[2-8] Transition metal hexafluorides, because of their simple high symmetry structure, are excellent systems in which to study this phenomenon.[6-10] Iridium hexafluoride is an important molecule in Jahn-Teller (JT) studies because its $(5d)^3$ electronic structure gives rise to a number of experimentally accessible degenerate and non-degenerate electronic states of the $(t_{2g})^3$ configuration. It is therefore possible to obtain detailed linear JT and general vibronic coupling[10] (GVC) information on a number of these excited electronic states. Additionally, the non-degenerate excited states serve as a built-in calibration for what might be considered "normal" non-JT behavior.

There have been several previous spectroscopic studies of IrF_6. These have included infrared absorption[11], Raman scattering[12], and visible-near infrared absorption spectroscopy[13]. Most of the studies have focused on the JT effect which is expected to occur in several of the $\Gamma_{8g}(O_h^\star)$ excited states. Experimental investigations have been encouraged and prompted by theoretical work on the dynamic JT effect in general[2-6] and its application to transition metal hexafluorides.[3,6,7,10]

The most extensive investigation of the visible and near IR absorption spectra of IrF_6 was done by Brand, Goodman, and Weinstock[13c] on gaseous and helium-cooled neat samples. However, their data were difficult to interpret for a number of reasons. The gas phase spectra are broad and exhibit typical rotational and hot band congestion. Neat crystal spectra have large band widths (ca. 30-50 cm^{-1} usually) which obscure much, if not all, of the sought after spectroscopic detail. The previous crystal spectroscopy is further

complicated by magnetic ordering[14], a low lying (5 cm^{-1}) electronic exciton band giving rise to excitonic hot bands[14], excited state electronic crystal field splitting, and two-particle host-guest transitions.[9,10]

The present work attempts to circumvent some of these difficulties by investigating mixed crystals of IrF_6 in either MoF_6, WF_6, or UF_6. Our previous study of ReF_6 crystal spectra lays the general foundation for the work presented in this paper.[9] A brief review of linear JT interaction theory, as it applies to MF_6 systems, can be found in reference 10. In this latter work we specifically discuss the consequences of two JT active vibrational modes and the effect of a low symmetry crystal field on transition metal hexafluorides. A symmetry-based GVC theory, applicable where the linear theory fails, is also discussed in reference 10.

After a brief review of the electronic, vibrational, and crystal properties of IrF_6, spectra dealing with transitions to the highest Γ_{7g} and Γ_{8g} ligand field $(t_{2g})^3$ states will be presented. The transition involving the Γ_{7g} Kramer's state will serve as a model for a "normal" (non-JT active) band.

II.   PROPERTIES OF IrF_6

A.   General

IrF_6 is a volatile molecular crystalline material. Important physical properties are listed in Table 1, along with those of the hexafluoride host materials used in this study. IrF_6 is paramagnetic and undergoes an anti-ferromagnetic phase transition ca. 9K.[15]

Crystal structures have been determined for the orthorhombic form of MoF_6[16] and UF_6[17]. Powder patterns have been obtained for several other hexa-fluorides including IrF_6.[18] The results indicate that the space group for hexafluorides in the low symmetry modification is D_{2h}^{16} (Pnma) with four mole-cules per unit cell at sites of C_s (m) symmetry.

B.   Vibrational States

The vibrations of an octahedral molecule such as IrF_6 are well known. A correlation diagram (Figure 1) shows the descent in symmetry from O_h to the site group C_s. The JT active vibrations are $v_2(e_g)$ and $v_5(t_{2g})$. The stretch-ing vibrations (v_1, v_2, v_3) are found in the 640-720 cm^{-1} region and the bend-ing modes (v_4, v_5, v_6) have energies around 200-300 cm^{-1}.

C.   Electronic States - $(5d)^3$ - $(t_{2g})^3$ Configuration

The deep yellow color of IrF_6 arises from what are believed to be dipole allowed charge-transfer transitions which begin at ~5000Å and continue to higher energy. Studies of MoF_6 and WF_6[19] indicate that these are ligand-to-metal charge-transfer transitions with an electron going to a metal $(dt_{2g})^n$ orbital.

The electronic states studied in this research are of the ligand-field variety.[13a] They derive from the combined action of a strong octahedral crystal field (10 D_q ~25,000 cm^{-1}), large spin-orbit coupling (ζ ~3400 cm^{-1})

4

and substantial electron-electron repulsion ($G \sim 2500$ cm^{-1}) in a $(5d)^3$ configuration.

Figure 2 shows how the predominantly $(t_{2g})^3$ orbitals split up under these interactions.[20] The present spectroscopic work deals with the highest Γ_{8g} ($^2T_{2g}$) state (E $\sim$14,900 cm^{-1}) and the Γ_{7g} ($^2T_{2g}$) state (E $\sim$12,100 cm^{-1}). It is important to note that the ground state degeneracy is mostly spin in character ($^4A_{2g}$), and therefore electric field-type perturbations should have a small effect on its energy and properties. Thus, in the ground state, JT effects are substantially reduced and the low-symmetry crystal potential produces little splitting (5 cm^{-1}) of this spin degeneracy.

III. EXPERIMENTAL

A. Absorption

Most of the data presented here were obtained from low temperature (4.2K and 1.6K), high resolution (0.1 cm^{-1}), visible and near infrared absorption spectra of mixed crystals of 0.25-3% IrF_6/MF_6 (M = U, Mo, W). Sample preparation techniques have been previously discussed.[9] Preliminary low resolution survey spectra were obtained on a Cary 14R. Tabulated data were taken either photographically on a 2.0 m spectrograph or photoelectrically on a 0.5 m double monochromator. For either detection scheme a GE 1958 or 1959 tungsten-iodide lamp, operated at constant current, was employed as th___ ___t source. Care was taken to filter as much of the light as possible ____vent sample heating; water filters were used to attenuate the low energy radiation and glass filters were used to attenuate the higher energies.

An Fe-Ne hollow cathode lamp was used as a wavelength standard.[21] Plates were measured with a Wild-Heerbrugg Stereocomparator to an accuracy of ±2.0 μm. Experimental lines were determined with a least squares polynomial fitting routine which gave a σ of about 0.02Å for sharp lines. Broad lines were measured to about ±0.2Å on a microdensitometer.

B. Emission

The experimental setup for monitoring emission consisted of an Ar^+ laser pumping a dye laser (rhodamine B), an f/6 double monochromator, and a cooled RCA C31034A photomultiplier tube operated in a photon counting mode. The sample was front surface irradiated to minimize self-absorption and effects of crystal quality. The Ar^+ laser pump power was ~7 watts at 5145Å which gave up to 1.2 watts of dye laser output with rhodamine B. Spectrometer slit widths were typically 100-200 μm.

6

IV. RESULTS AND DISCUSSION

A. Γ_{7g} ($^2T_{2g}$) Transition (12,100 cm^{-1}) - Absorption

The Γ_{7g} transition [$\Gamma_{7g} \leftarrow \Gamma_{8g}$ ($^4A_{2g}$)] is discussed first since it is the least complicated of all the IrF$_6$ d-d transitions. The Γ_{7g} state is a well isolated Kramer's doublet. Free from complications due to intra-state vibronic coupling and spatial electronic degeneracy, other effects, such as site splitting of degenerate vibrations ($\nu_2,\nu_3,\nu_4,\nu_5,\nu_6$), two-particle states, and anharmonicities, can be studied at high resolution in uncongested spectra. We use this band as a model for the interpretation of the system $\Gamma_{8g} \leftarrow \Gamma_{8g}$ at 14,900 cm^{-1} and as an indication of IrF$_6$ behavior in the C$_s$ crystal site.

The Γ_{7g} spectrum is typical of a g-g parity forbidden transition: its overall intensity is low and much of it is vibronically-induced by the odd vibrational fundamentals. It should be noted that the borrowed vibronic intensity is small in an absolute sense since the oscillator strength of each vibronic peak is only on the order of 10^{-6}. However, due to the low symmetry crystal field, the origin is much more intense than observed in the gas phase[13]; in fact, as can be seen in Figure 3a, the origin intensity is of the same order of magnitude as the vibronic peaks. The even fundamentals ν_2 and ν_5 are located, but are weak; their intensities are apparently crystal-induced. A short Franck-Condon progression in ν_1 is observed (n $\leq$ 2) and is indicative of little change in geometry upon excitation.

Moderate to weak intensity combinations, after both the bending (ν_4,ν_5,ν_6) and stretching (ν_1, ν_2, ν_3) regions, are also observed. In general, all binary combinations of odd and even modes are found. Of particular interest are the ($\nu_i + \nu_2$) and ($\nu_i + \nu_5$) combinations which are potentially JT active in a Γ_{8g} state (see Table 2). Observation of such states can help verify ν_5 and ν_2 assignments in situations for which their fundamentals are obscured

or greatly changed in frequency from their ground state values.

Two-particle host-guest transitions[9], some of moderate intensity, appear near single particle guest bands. These transitions are most readily recognized by their large line widths and, of course, their host-to-host variation (see Table 2).

Since the concentrations of IrF_6 used here are relatively high (0.25 - 3.0%), pair structure is seen, mainly around the 0-0 transition. The behavior of the features is found to be similar to those reported previously for ReF_6 mixed crystals.[9]

Most of these general comments can be verified from the low resolution survey spectra presented in Figure 3a. Table 3 contains a detailed listing of these transitions from high resolution data for IrF_6/MoF_6. [Complete data for other systems (IrF_6, IrF_6/UF_6, IrF_6/WF_6) have also been obtained, but they add little to that listed in Table 1. When such information is needed in the discussion, it will be listed in the text or in summary tables.]

Vibrational site splittings are found to be of the order of 5 cm^{-1}. Since the electronic states arising from the $(t_{2g})^3$ configuration are similar, it is expected that these site splittings are representative of those in other excited $(t_{2g})^3$ electronic states as well. They are also close to site splittings found for the ground and excited states of ReF_6 in these host systems.[9,10,22] The data are summarized in Table 4. An interesting feature of the ν_6 site splitting pattern is illustrated in Figure 4. The low energy component of ν_6 in IrF_6/WF_6 is much weaker than the other two. However, in the hot band transition to ν_6 (see Table 5) at 5.7 cm^{-1} lower energy, the intensity pattern is reversed. This latter transition involves the upper component of the crystal field split degenerate ground Γ_{8g}-state. The unexpected intensity pattern arises from polarization properties of the transition. Based on these

hot bands, it is clear that all three components are part of the same vibrational structure.

Two-particle transitions, often of substantial intensity, are observed throughout the bending region. In general, they are easily assigned based on their width and the known host ground state vibrational exciton bands.[22] Nonetheless, they can drastically change the appearance of the spectra. A particularly striking example of this arises for the case of exact resonance between single and two-particle transitions, as occurs for IrF_6 $[\Gamma_{7g} + \nu_6]$ in a UF_6 host $[\Gamma_{7g} + \nu_5 (UF_6)]$. Comparison of the IrF_6/WF_6 and IrF_6/UF_6 spectra in the bending region (see Figures 4b and 5) illustrates this point clearly. In a mixed crystal of IrF_6/UF_6, the $[\Gamma_{7g} + \nu_6] \leftarrow \Gamma_{8g}$ transition is quite broad compared to its counterpart in IrF_6/WF_6, due to the resonance in the former crystal.

The most important observation made in the bending region is the direct location for the first time of $\nu_5(t_{2g})$ at 285.3, 286.3, and 289.4 cm^{-1} (IrF_6/MoF_6), 285.0, 285.7, 288.6 cm^{-1} (IrF_6/WF_6), and 285.0, 285.7, 289.0 cm^{-1} (IrF_6/UF_6) above the origin. The Γ_{7g} ν_5 is 20 cm^{-1} higher in energy than that found in the Γ_{8g} ground state (see Table 6).

The stretching region (ν_1, ν_2, ν_3) is somewhat more complex than the bending region due to two-particle transitions and combinations and overtones of IrF_6. As can be seen in Figures 6 and 7, the broad feature at 765 cm^{-1} in the IrF_6/MoF_6 spectrum has no counterpart in the IrF_6/UF_6 spectrum. This is, of course, a strong indication for a two-particle host-guest transition.

In the IrF_6/WF_6 spectrum, the corresponding feature occurs at 735 cm^{-1}. The exact assignment of this feature (see Table 2) is not entirely obvious but $3\nu_4(h)$ seems to fit well with host energetics. This combination has not been observed in the infrared but $2\nu_4(h)$ has been observed in the Raman spectrum[22] and exhibits enough anharmonicity to account for the observations. Aside from this particular resonance there is little other intensity in the two-particle spectrum higher in energy than ~750 cm^{-1} past the origin. There is evidently especially good overlap between $3\nu_4(h)$ and ν_3(guest).[9]

In addition to ν_1 and ν_3 identified in this region, we have directly observed ν_2, for the first time, at 713.0 and 717.7 cm^{-1} (IrF_6/MoF_6), 708.3 and 716.9 cm^{-1} (IrF_6/UF_6), and 712.8 and 718.1 cm^{-1} (IrF_6/WF_6) above the origin. This is roughly 70 cm^{-1} higher in energy than ν_2 in the ground state; therefore, justification for this assignment is appropriate. There are only two other possibilities for alternate assignments of this doublet: intensified, through resonance with ν_3, ternary combinations or overtones (e.g., $2\nu_6 + \nu_6$) and components of ν_3 itself. The former possibility seems unlikely based on line shapes and the number of expected peaks for such transitions. ν_3 is seen to split in IrF_6/UF_6 crystals and yields a 1.9 cm^{-1} overall site splitting with roughly the expected intensity distribution. Since UF_6 is the most distorted host system[9,10,22], we would not expect large ν_3 site splittings in the other mixed crystals. Thus, both of these alternative suggestions for the ν_2 assignments can be rejected.

Additionally, it is interesting to note that the ν_2 site splitting (Table 4) in UF_6, 8.6 cm^{-1}, is roughly twice as big as in other host crystals. This correlates with the increased UF_6 crystal distortion in the $e_g(\theta)$ coordinate with respect to either WF_6 or MoF_6.[16,17]

Direct support for both the ν_2 and ν_5 assignments comes from combination bands. All binary combinations of odd and even vibrations have been observed except (ν_4 + ν_2). Thus three combinations for ν_2 and four combinations for ν_5 have been identified. These clearly indicate that the fundamental modes are even and that they have rough energies of 715 and 285 cm^{-1}, respectively.

The cause of the +70 cm^{-1} shift in ν_2 energy from the ground Γ_{8g} state to the excited Γ_{7g} state is not certain. It is probably not simply associated with the difference in electronic states since the next largest change for a vibrational frequency is -28 cm^{-1} for ν_3 (see Table 6). More likely, the large shift is due to vibronic coupling within the $(t_{2g})^3$ electronic manifold. The coupling can be viewed as a pseudo-Jahn Teller (PJT) interaction, the reference degenerate state being the highly degenerate $(t_{2g})^3$ configuration present before electron-electron repulsion and spin-orbit perturbations are applied. Since the parameter governing this PJT effect is related to the JT parameters in the Γ_{8g} states, a large ν_2 shift would imply that a large ν_2 JT interaction exists in one or more of the Γ_{8g} states.

The above analysis of the non-JT active Γ_{7g} electronic state can now serve as a point of departure for the analysis of the JT-active Γ_{8g} state at 14,900 cm^{-1}. We can look for changes in the fundamental frequencies of ν_2 and ν_5 as well as combinations of these vibrations with the vibronic origins ν_3, ν_4 and ν_6. In general, these fundamentals and combinations can be both split and shifted by the vibronic perturbation.

To summarize our findings for the $\Gamma_{7g} \leftarrow \Gamma_{8g}$ ($^4A_{2g}$) absorption band, several important observations have been made:

1)   Vibrational site splitting is generally about 5 cm^{-1}.

2) ν_5 (~285 cm^{-1}) and ν_2 (~715 cm^{-1}) have been located.

3) ν_1, ν_2 and ν_5 form combinations with the odd vibronic origins ν_3, ν_4 and ν_6.

4) The ν_5 vibrational frequency is shifted +20 cm^{-1} to higher energy with respect to its ground state frequency. The ν_2 vibrational frequency is shifted +70 cm^{-1} in the same direction with respect to its ground state value. Such shifts may be associated with a PJT coupling within the $(t_{2g})^3$ electronic configuration.

5) Two-particle states broaden vibronic states with which they interact, especially in the case of an exact resonance.

6) Two-particle transitions are evident in the fundamental region, but are not as prominent as expected in the combination regions. Apparently overlap between single particle and two-particle vibronic transitions is not as large for guest combinations as it is for guest fundamentals.

B. $\Gamma_{8g}(^2T_{2g})$ Transition (14,900 cm^{-1}) - Absorption

In a number of respects, the $\Gamma_{8g}[\Gamma_{8g}(^2T_{2g})\leftarrow\Gamma_{8g}(^4A_{2g})]$ band is similar to the Γ_{7g} band just discussed; the transition is parity forbidden, giving rise to prominent vibronic false origins (ν_3, ν_4, ν_6). The overall intensity pattern found here is similar to that discussed for the Γ_{7g} transition. However, there are also a number of conspicuous differences: a) due to the low symmetry crystal field, the excited Γ_{8g} state splits into two components, both of which are Kramer's pairs--the origin and all vibronic components carry this splitting; b) many peaks in the spectrum are much broader than their counterparts in the Γ_{7g} transition (compare Figures 8 and 9 with Figures 4 and 5); and c) there is a good deal of intensity in this transition in the region past 1,000 cm^{-1} from the 0-0 band.

The origin is somewhat complicated by the presence of pair and

phonon structure. Both of these additional features are straightforward to identify from concentration dependence (0.1 - 1.0% IrF_6/XF_6), line widths, and existing Raman scattering data on host system phonons.[22]

The crystal field splitting of the origin varies from 30-70 cm^{-1} depending on host crystal (Table 5) and thus phonons built on origin (a) can be in resonance with origin (b). As is evident from Table 7, origin (b) seems to enhance the intensity of nearby phonons (built on origin (a)). The effect is most pronounced in UF_6 for which phonons appear to have more intensity than origin (b), and it seems almost absent in WF_6, apparently because origin (b) (46.3 cm^{-1} from origin (a)) falls in a gap in the phonon structure. A reasonable explanation of this enhancement is that these phonon bands are two-particle states (origin (a) plus lattice mode) which interact with the near-resonant single particle state, origin (b).

It is expected within the framework of the Born-Oppenheimer approximation that non-JT active vibrations (ν_1, ν_3, ν_4, ν_6) will build on each of these origins independently and therefore the origin crystal field splitting will be preserved for vibr   c transitions. Figures 8, 9, and Table 7 make this interpretation quite   ous. This situation is, however, more complex for the JT active modes   g) and $\nu_5(t_{2g})$. Since crystal field and JT terms are roughly expected to be of comparable magnitude, their effects must be considered simultaneously.[10] Depending on their relative strengths and (approximate) symmetries, these two perturbations can either operate more or less independently, one can quench the other, or their behavior can be inextricably coupled.

The bending region (ν_4, ν_5, ν_6) for IrF_6/WF_6 and IrF_6/MoF_6 is shown in Figures 8 and 9, respectively. It is apparent that two-particle transitions contribute significantly to the spectra in this region since the two traces

look quite different. Between 225 and 350 cm^{-1} above the origin, the Γ_{8g} transition is much broader than the comparable portion of the Γ_{7g} band. The reason for the increased width, however, is clear: the interaction of two-particle and single particle vibronic states. These states can be built on either origin and thus the chances of a near or exact resonance are substantial.

Once two-particle features are recognized and their line width perturbations are understood, the assignment of the bending region becomes possible. A general assignment of this part of the spectrum is given in Figures 8 and 9 and detailed numbers are presented in Table 7. The advantages of using a few different host materials in the study becomes quite apparent particularly in the $\nu_4(a,h)$ [ν_4 of the host built on the lower energy (a) origin] and $\nu_4(b,h)$ regions.

The odd vibrations ν_6 and ν_4 are readily located by their energy and high intensity. Site splittings of the individual modes built on the (a) or (b) origins are more difficult to characterize due to the broadening effects of the two-particle transitions, particularly starting at about 250 cm^{-1} above origin (a). This effect is readily apparent from Figures 8 and 9. Because ν_6 is below 250 cm^{-1}, a small site splitting of 2.4 cm^{-1} (compared with 4.4 cm^{-1} in the Γ_{7g} band) has been assigned for ν_6 of IrF_6/MoF_6.

Once ν_4, ν_6 transitions have been assigned and two-particle features are isolated, remaining bending intensity can be associated with ν_5. Pending corroboration from overtone and combination data (given below), we can assign 202.7, 208.9, and 241.5 cm^{-1} ($\nu_5^{1,2,3}$) peaks as the three components of $\nu_5(a)$. The $\nu_5(b)$ peaks are found at the origin crystal field splitting energy from their $\nu_5(a)$ counterparts. Although the $\nu_5(b)$ peaks are not as obvious as those of $\nu_5(a)$ due to two-particle interference, they can be observed in combinations built on ν_1. This assignment of ν_5 will be discussed below at

some length. It should be compared with $\nu_5(\Gamma_{7g})$ transitions at <u>ca.</u>
285, 286, and 289 cm^{-1} and ν_5 ground state at ~265 cm^{-1}.

The (ν_4, ν_5, ν_6) combination region (400-600 cm^{-1}) contains important
information on ν_5. The best data available are for the IrF$_6$/MoF$_6$ mixed
crystal; these will be discussed here but they are corroborated by both neat
and other mixed crystal spectra. Confirmation of above $\nu_5^{1,2,3}$ assignments
is found in the $\nu_4 + \nu_5^{1,2,3}$ combinations. The first ν_5 overtone is also
observed in this region and is tabulated in Table 7. Since, in terms of
width and intensities, these spectra are almost identical to the comparable
region in the Γ_{7g} band, we find this very compelling evidence for the $\nu_5^{1,2,3}$
assignment.

The (ν_1, ν_2, ν_3) stretching region seems less congested by two-particle
transitions. The totally symmetric ν_1(a) is identified as a single sharp
peak. It serves as an origin for many combination bands. ν_3 is recognized
as the most intense feature in this region (actually, the entire spectrum)
and it serves as a false origin. Conspicuously missing from the spectrum is
ν_2. A moderate JT interaction should give ν_2 substantial intensity, parti-
cularly since it was observed as a fundamental in the Γ_{7g} band at <u>ca.</u> 713
and 717 cm^{-1}. It may well be masked by two-particle transitions and frequency
shifts. For IrF$_6$/MoF$_6$ or WF$_6$, no observed features can be uniquely assigned
to ν_2 or any of its combinations or overtones. The $3\nu_4$(a,h), $3\nu_4$(b,h) peaks
are also found in the IrF$_6$/MoF$_6$ and WF$_6$ spectra, in analogy with the Γ_{7g} band.

On the other hand, in IrF$_6$/UF$_6$, a peak at 716.0 cm^{-1} is tentatively
assigned as a component of ν_2. The reason that these peaks show up only in
the UF$_6$ host crystal and not the others is likely associated with the differ-
ence in two-particle interactions and intensities. The larger (by a factor
of two) crystal field splitting in UF$_6$ also contributes to the reduced crowding

and overlapping intensity in this region. For example, IrF_6 ($\nu_2 + \nu_5$),
observed in IrF_6/UF_6 mixed crystals, may be obscured in both MoF_6 and WF_6 by
($\nu_1 + \nu_5(b)$). Since ν_2 has two components and we have tentatively assigned
only one of them, it is difficult to comment extensively on the JT nature of
ν_2. However, it   ted that ν_2 is weak (weaker than ν_5) and that the
one tentatively obs   ponent falls in the region expected based on a
comparison with the non-JT active Γ_{7g} state.

One of the more prominent features in the Γ_{8g} spectrum appears at origin
(a) plus 1024 cm^{-1} (15,907.3 cm^{-1} for IrF_6/MoF_6). It is also observed in the
gas phase[13] as an intense transition; it has no counterpart in any of the
other electronic d-d transitions for IrF_6 (i.e., Γ_{7g} 0.8 μm, Γ_{8g} 1.2 μm,
Γ_{8g} 1.6 μm).[14] It is different from any band appearing in the Γ_{8g} transitions
in the following two ways: it has no crystal field splitting and broad peaks
of medium to weak intensity occur 20-150 cm^{-1} to its high energy side. These
latter transitions are probably not two-particle peaks based on a comparison
with the Γ_{7g} band. Because of their line shapes, intensities, and energies,
these transitions are assigned as phonon additions to the 1024 cm^{-1} peak.
In view of the above experimental findings we have assigned the 15,907.3 cm^{-1}
peak as a new electronic origin of Γ_{6g} or Γ_{7g} symmetry. Since there are no
missing $(t_{2g})^3$ ligand field states, this origin must belong to an even charge-
transfer state.

Two further pieces of evidence are at least consistent with this present
assignment. There are broad features in the region 500-700 cm^{-1} away from the
new electronic origin which do not fit into the Γ_{8g} transition. These features
are good candidates for the stretching modes (ν_1, ν_2, ν_3) in the charge-transfer
state, their width being characteristic of inter-configurational transitions
and their unrecognizable energies being associated with the large change in

electronic distribution in the new state. Their intensity is of comparable magnitude to the vibronic peaks in the Γ_{8g} and Γ_{7g} transition. One would then expect to see $2(\nu_1', \nu_2', \nu_3')$ and weak peaks are indeed observed in the region 1000-1400 cm^{-1} to higher energy than this new origin.

The other indication that the 1024 cm^{-1} IrF_6/MoF_6 feature is indeed a new electronic state comes from gas-to-crystal shift data. The new electronic state has a consistently larger (by about 15 cm^{-1}) shift than the Γ_{8g} state and the difference between the ν_3 and the 1024 cm^{-1} band varies throughout the series by ± 10 cm^{-1}. While these differences are not as large as one might expect, they are about a factor of two or three larger than other comparable changes in the series IrF_6, IrF_6/WF_6, UF_6, MoF_6 for known Γ_{8g} components.

It is important to point out that the above assignments differ greatly from those of previous workers.[13b,c] The 1024 cm^{-1} peak had been assigned as $(\nu_3 + \nu_5 \ (\frac{1}{2}))$ and the $n(\nu_1', \nu_2', \nu_3')$ peaks were assigned as $(\nu_3 + \nu_2(\frac{1}{2}))$ and $(\nu_3 + 2\nu_2(\frac{1}{2}))$ for n = 1 and 2 respectively. The previous reduction scheme relied heavily on the linear JT theory for a single active mode.[7,8] This interpretation cannot be correct in light of the present work since: a) the three expected ν_5 components are all observed, none of which lies at 300 cm^{-1} as would be required; b) each of these three ν_5 components has a crystal field partner while the 1024 cm^{-1} peak does not; and c) ν_2 has been tentatively identified at ~715 cm^{-1}.

A further possibility for the 1024 cm^{-1} feature is that it is ν_2 itself, raised in energy by a strong JT interaction. We have rejected this possibility based mostly on our previous calculations presented in part in references 9 and 14. We have shown that for a tetragonal crystal field potential ν_5 preserves the origin splitting (ca. 40 cm^{-1}) but ν_2 would quench it. Thus, the absence of crystal field splitting does not a priori eliminate this feature as a candidate for ν_2. However, when the coupled ν_2-ν_5 JT problem is simul-

taneously diagonalized with $\nu_2^0 \sim 710$ cm^{-1} and $\nu_5^0 \sim 285$ cm^{-1}, it is not possible to raise ν_2 above 900 cm^{-1} even for JT parameters D_2 and D_5 greater than 1.5. Initially ν_2 increases in energy but then anticrossing interactions with higher "overtones" begin to depress it. Additionally, such large D_2 and D_5 parameters would yield long intense progressions in these modes, which are not clearly observed. Thus, the possibility of such an assignment seems remote. The inclusion of second order terms for ν_2 (GVC) does not appear to change these general conclusions.[23]

Summarizing our results for the $\Gamma_{8g} \leftarrow \Gamma_{8g}$ transitions, it was found that many of the main features of this band are like those found in the $\Gamma_{7g} \leftarrow \Gamma_{8g}$ transition. The origin is observed, ν_6, ν_4, ν_3 serve as vibronic origins, and most odd-even combinations are identified. The difference between these two transitions arises from the JT nature of the excited Γ_{8g}-state and the location of a new electronic Γ_{7g} or Γ_{6g} low-lying charge transfer state. This latter feature has no counterpart in any of the other Γ_{8g}, Γ_{7g}, or Γ_{6g} transitions in this molecule.[14] The ν_5 transition is clearly involved in vibronic interaction as it is shifted from its expected value of 285 cm^{-1} and split. All observed features, with the exception of those associated with the new state, carry a ~ 30 (neat IrF$_6$) to ~ 70 (UF$_6$) cm^{-1} crystal field splitting arising from removal of the degeneracy of the electronic origin.

C.   Emission

The three important observations for the Γ_{8g} spectrum (location of ν_5, absence of significant and positively identifiable ν_2 intensity, and the assignment of a new electronic origin) would be further corroborated and verified by the appearance and assignment of a well-resolved emission spectra from the Γ_{7g}, Γ_{8g}, and new ("charge transfer") state. Since the other $5d^3$

systems, such as $ReBr_6^{-2}$ and $ReCl_6^{-2}$ emit strongly,[24,25] it was thought that IrF_6 might, as well. However, only very weak emission was observed with either dye laser excitation from 6800Å to 5800Å (~1.2 watts) or argon laser excitation at 5145 or 4880Å (>5 watts). Only one emission line was observed under conditions of dye laser excitation, [origin-ν_3] at about 80 cps. To emphasize just how weak this emission is, the unfocused dye laser (3 mm beam) also pro-duced an IrF_6 ν_1 Raman scattering of 300 cps in a 0.5% IrF_6/UF_6 crystal. The emission to ν_3 was always based on the Γ_{8g} (0,0) while the IrF_6 ν_1 Raman scattering, of course, followed the laser frequency exactly. Excitation at 15,907.3 cm^{-1} for IrF_6/MoF_6 (Γ_{8g} (0,0) + 1024.0 cm^{-1}) also produced emission identical to that described above. Emission spectra were thus not useful in the assignment of the 6800Å-5500Å Γ_{8g}-Γ_{7g} (Γ_{6g}) charge transfer region of the IrF_6 spectrum.

V. JAHN-TELLER INTERPRETATION OF THE Γ_8 $(^2T_{2g})$ STATE

Observations in the $\Gamma_{8g} \leftarrow \Gamma_{8g}$ transition that pertain to an intra-state vibronic coupling (JT or GVC) interpretation are the following:

a) Substantial splitting of the ν_5 components (for IrF_6/MoF_6: 202.7, 208.9 and 241.5 cm^{-1}).

b) Large shift in the center-of-gravity of $\nu_5(\Gamma_{8g})$ $[\nu_5^0 \sim 218\ cm^{-1}]$, from an "expected" value of $\sim 285\ cm^{-1}$ (the ν_5 frequency observed in the Γ_7 state).

c) Preservation of the origin crystal field splitting for the ν_5 components.

d) Observation of non-harmonic overtone of ν_5 (for IrF_6/MoF_6: 416.6, 419.1, 452.3, 461.4 cm^{-1}) of considerably less intensity than the fundamental.

e) Little evidence of ν_2.

While most of these observations can be understood either based on a coupled ν_2-ν_5 linear JT interaction[10] $[\Gamma_8 \times (e_g + t_{2g})]$ or based on quadratic or higher order terms (GVC) in the vibronic Hamiltonian, alternate approaches to the above ν_5 observations might be appropriately considered before proceeding further. The shift in ν_5^0 could be attributed simply to differences in the electronic states $(\Gamma_{8g}, \Gamma_{7g})$ or perhaps strong vibronic coupling to the nearby charge transfer states. (Note that vibronic coupling to lower energy states could not depress ν_5^0.) Observation (a), dealing with ν_5 splitting, is then explained by the usual linear JT theory with a splitting parameter D_5 of ~ 0.03, the $j_5 = 3/2$ level being at 202.7 and 208.9 cm^{-1} and the $j_5 = 1/2$ level being at 241.5 cm^{-1}. The residual splitting of the $j_5 = 3/2$ level might be explained as a site splitting. ─────────────────────────────

However, this explanation is not satisfactory for several reasons. It does not seem reasonable that ν_5^0 would change so much from the Γ_{7g} to the Γ_{8g} state while the other vibrations change so little. It also seems more reasonable to look for an intra-state vibronic coupling mechanism for (b) since a similar shift is seen for ν_2^0 in ReF_6[10] and for ν_5^0 in the Γ_8 $(^2T_1)$ of IrF_6.[13c,14]

The coupled $\nu_2-\nu_5$ $[\Gamma_8 \times (e_g + t_2)]$ JT model[10] provides a plausible explanation for the apparent shift in ν_5^0. In this model ν_2 and ν_5 interact such that the $j_5 = 1/2$ level is strongly repelled by the ν_2 levels. The $j_5 = 3/2$ is only weakly perturbed by this coupling. However, since little information is available for ν_2, it is difficult to assess the importance of this mechanism.

Another intra-state vibronic coupling mechanism which can explain the observations involves addition of quadratic (and possibly higher order) terms to the vibronic Hamiltonian (GVC). For a t_{2g} vibration, there are three different types of quadratic terms: that is, the symmetric direct product of t_{2g} coordinates, $[t_{2g}]^2$, contains a_{1g}, e_g, and t_{2g}. The quadratic vibronic terms can be labelled by these vibrational symmetries and are designated as $Q(a_{1g})$, $Q(e_g)$, and $Q(t_{2g})$.

A qualitative understanding of the effect of these additional terms can be gained via the GVC theory.[10] Figure 10 illustrates the "descent-in-symmetry" of ν_5 in a Γ_8 state from the Born-Oppenheimer limit, for which high degeneracy exists, through the linear JT regime for which a pseudo-spherical symmetry preserves extra degeneracy, to the rigorous symmetry labels of the point group, O_h^*, which are necessary when quadratic (or higher order) terms are present. It can be seen that the $j_5 = 3/2$ level is split by this perturbation while the $j_5 = 1/2$ level is not.[23]

Observations in the Γ_{8g} state would then be explained in the GVC model as follows: the shift in ν_5^0 is mainly due to the $Q(a_{1g})$ term; the larger splitting in the ν_5 components is due to the linear JT term, $D_5 \sim 0.03$; and the smaller splitting is due to the combined action of $Q(e_g)$, $Q(t_{2g})$ and site splitting terms. The non-harmonic overtone of ν_5 is consistent with this vibronic coupling interpretation; the relatively small intensity is consistent with the above linear JT parameter. A detailed calculation for $[\Gamma_{8g} \times \nu_5]$ has not been carried out in the combined JT and GVC model, however, due to its complexity. Four variable parameters (D_5, $Q(a_{1g})$, $Q(e_g)$, $Q(t_{2g})$) would be required for such a calculation, and the limited ν_5 data do not warrant a general fitting procedure. A simpler quadratic calculation involving ν_2 (e_g) has been done and the qualitative behavior described above is found.[23]

Both proposed intra-state vibronic coupling mechanisms, GVC and ν_2-ν_5 linear JT coupling, seem capable of explaining the data, and it is probable that both contribute.

Finally, it should be noted that the appearance of the origin crystal field splitting on the $n\nu_5$ levels is consistent with an approximate crystal field symmetry of D_{4h} and not with D_{3d} or lower symmetry.[10] The relevant theory has been worked out in detail for $[(\Gamma_8 + \Phi(D_{4h})) \times t_{2g}]$,[10] but not for the complex situation found important here, i.e., coupled ν_2-ν_5 linear JT and quadratic (mainly $Q(a_{1g})$) interactions. However, the following qualitative ideas are helpful in understanding the situation. The coupled ν_2-ν_5 linear JT interaction probably could cause a quenching of a D_{4h} crystal field, due to mixing in of ν_2 character into the ν_5 wavefunctions, but the $Q(a_{1g})$ quadratic term should preserve the D_{4h} crystal field splitting. The smaller $Q(e_g)$ and $Q(t_{2g})$ terms should have negligible effect in this context. Apparently,

the magnitude of the ν_2-ν_5 linear JT interaction is not sufficient to cause an identifiable quenching of the approximate D_{4h} crystal field.

VI. CONCLUSIONS

The main conclusion to be drawn from this work is that a dynamic JT interaction is present in the $n\nu_5$ modes of the Γ_{8g} electronic state, but that it is not well characterized by the usual (linear) JT theory. To this latter theory must be added coupling between different JT active modes (i.e., ν_2 and ν_5) and quadratic GVC terms.

Additional conclusions reached are:

a) A new electronic state has been located at 15,900 cm^{-1}; it is of Γ_{6g} or Γ_{7g} (O_h^*) symmetry and probably charge transfer in nature.

b) In nearly degenerate electronic states, two-particle states associated with one electronic origin can interact with transitions built on the other origin. Consequently, two-particle transitions play a much more dominant role in the spectra of nearly degenerate states (i.e., Γ_{8g} split by a low symmetry crystal field potential) than they do in the spectra of a non-degenerate state.

c) The ν_2 and ν_5 vibrational frequencies in the Γ_{7g} electronic state are significantly shifted in energy from their ground state values. This shift has been attributed to a possible pseudo-Jahn Teller interaction with the other $(t_{2g})^3$ states.

References

1. H. A. Jahn, E. Teller, Proc. Roy. Soc. A161, 220 (1939) and H. A. Jahn, Proc. Roy. Soc. A164, 117 (1938).

2. W. Moffitt, A. D. Liehr, Phys. Rev., 106, 1195 (1957).

3. W. Moffitt, W. Thorson, Phys. Rev., 108, 1251 (1957).

4. H. C. Longuet-Higgens, U. Opik, H. M. L. Price and R. A. Sack, Proc. Roy. Soc., A244, 1 (1958).

5. H. C. Longuet-Higgens, Adv. Spec., 2, 429 (1961).

6. W. Thorson, W. Moffitt, Phys. Rev., 168, 362 (1968).

7. B. Weinstock, G. L. Goodman, Adv. Chem. Phys., IX, 169 (1965).

8. R. Englman, "The Jahn Teller Effect in Molecules and Crystals", Wiley & Sons, (NY, 1972).

9. E. R. Bernstein and G. R. Meredith, J. Chem. Phys., 64, 375 (1976).

10. G. R. Meredith, J. D. Webb, and E. R. Bernstein, Mol. Phys., ___ (1977).

11a. H. C. Mattraw, N. J. Hawkins, D. R. Carpenter, and W. W. Sabol, J. Chem. Phys., 23, 985 (1955).

11b. H. H. Claassen, B. Weinstock, J. Chem. Phys., 33, 436 (1960).

12. H. H. Claassen, H. Selig, Israel J. Chem., 7, 499 (1969).

13a. W. Moffitt, G. L. Goodman, M. Fred, and B. Weinstock, Mol. Phys., 2, 109 (1959).

13b. J. C. D. Brand and G. L. Goodman, Can. J. Phys., 46, 1721 (1968).

13c. J. C. D. Brand, G. L. Goodman and B. Weinstock, J. Mol. Spec., 37, 464 (1971).

14. E. R. Bernstein and J. D. Webb, unpublished results.

15. B. Weinstock, E. F. Westrum, Jr., and G. L. Goodman, Proc. Int. Conf. Low Temp. Phys. (London), 405 (1962).

16.   J. H. Levy, J. C. Taylor, and P. W. Taylor, Acta Cryst. $\underline{B31}$, 398 (1975).

17.   J. C. Taylor, P. W. Wilson, and J. W. Kelly, Acta Cryst. $\underline{B29}$, 7 (1973).

18.   S. Siegel and D. A. Northrop, Inorg. Chem., $\underline{5}$, 2187 (1966).

19.   R. McDiarmid, J. Mol. Spec., $\underline{39}$, 332 (1971); J. Chem. Phys., $\underline{61}$, 3333 (1974).

20.   W. A. Runciman and K. A. Schroeder, Proc. Roy. Soc. (London), $\underline{A265}$, 489 (1962).

21.   H. M. Crosswhite, J. Res. Nat. Bur. Stand., $\underline{79A}$, 17 (1975).

22.   E. R. Bernstein and G. R. Meredith, Chem. Phys., ___, (1977).

23.   E. R. Bernstein and J. D. Webb, Mol. Phys., to be published.

24.   A. M. Black and C. D. Flint, J. C. S. Faraday II $\underline{71}$, 1871 (1975).

25.   A. R. Reinberg, S. G. Parker, Phys. Rev. $\underline{B1}$, 2085 (1970).

Table 1.   Physical Properties of Some Transition Metal Hexafluorides.

Molecule	Metal-Fluorine Distance (Å)	Vapor Pressure at 300K (Torr)	Solid Transition T(°C)	ΔS(eu)	Fusion T(°C)	ΔS(eu)	Vaporization T(°C)	ΔS(eu)
IrF_6	1.830^a	246^c	+0.4	6.21^c	44.0	3.74^c	54	22.6^c
MoF_6	1.820^b	584^c	-9.67	7.41^e	17.58	3.56^e	34	22.5^c
WF_6	1.833^a	1008^c	-8.5	7.81^f	2.0	3.56^f	17	21.8^c
UF_6	1.996^a	127^d	--	--	64.05	13.61^g	64.05	20.2^g

a. M. Kimura, V. Schomaker and D. W. Smith, J. Chem. Phys., 48 (9), 4001 (1968).

b. H. Seip, Sel. Top. Struct. Chem., 1967, 26, (1967).

c. G. H. Cady and G. B. Hargreaves, J. Chem. Soc. (London), 1961, 1563 (1961).

d. G. D. Oliver, H. F. Milton and J. W. Grysard, J. Am. Chem. Soc., 75, 2827 (1953).

e. D. W. Osborne, L. Shreiva, J. G. Malm, H. Selig and L. Rochester, J. Chem. Phys., 44, 2802 (1966).

f. E. F. Westrum, Jr., J. Chem. Phys., 63, 47 (1966).

g. B. Weinstock, Rec. Chem. Prog., 23, 23 (1962).

Table 2. Range of $\underline{k} = 0$ components for neat MF_6 crystals[a]. Serves as an approximation for location and width of density of state functions observed in two-particle transitions in IrF_6/MF_6 mixed crystals.

	ν_1	ν_2	ν_3	ν_4	ν_5	ν_6	$2\nu_4$
UF_6	663.9	510-534	586-649	175-197	206-229	146-163	374
WF_6	772.2	669-675[b]	678-698[b]	240-265	320-328	147	465
MoF_6	742.2	642-652	694-721[c]	247-275	316-324	140	498-526

a. E. R. Bernstein and G. R. Meredith, Chem. Phys. __,   (1977).

b. ν_2 and ν_3 are interacting band. See reference a.

c. ν_3 predicted (reference a) to extend to ~760 cm^{-1} but obscured by ν_1.

Table 3. Summary of $\Gamma_7(^2T_{2g})$ absorption spectrum of mixed crystals of IrF_6/MoF_6 at 1.8K. Frequencies are given in cm^{-1}. Frequency uncertainty is ± 0.1 cm^{-1} for sharp lines.

Intensity[a]	FWHM (cm^{-1})[b]	Vacuum Wavenumbers (cm^{-1})	$\Delta\nu(\text{origin})$ (cm^{-1})	Assignment
--	--	12087.6	-8.5	
--	--	12088.0	-8.1	
--	--	12088.8	-7.3	Pairs
--	--	12089.8	-6.3	
--	--	12090.8	-5.3	hb of origin[c]
--	--	12092.4	-3.7	
--	--	12093.0	-3.1	
--	--	12093.9	-2.2	Pairs
--	--	12095.0	-1.1	
--	--	12095.4	-0.7	
S	1.0	12096.1 (8264.88Å)	0.0	Origin
--	--	12097.2	1.1	
--	--	12098.1	2.0	
--	--	12098.8	2.7	
--	0.3	12099.5	3.4	Pairs
--	0.3	12100.6	4.5	
--	0.3	12101.1	5.0	
--	0.3	12102.1	6.0	
--	0.3	12105.3	9.2	
W	10	12135.0	38.9	
W	5	12146.0	49.9	
W	7	12156.5	60.4	Phonons
W	5	12165.5	69.4	
W	3	12171.6	75.5	
W	5	12176.1	80.0	
W	15	12244.1	148.0	$\nu_6(h)$[d]
W	1	12306.1	210.0	hb of ν_6
W	1	12308.5	212.4	hb of ν_6
M	1	12311.4	215.3	
S	1	12313.7	217.6	ν_6
S	1	12315.8	219.7	
W	--	12351.2	255.1	
W	5	12353.9	257.8	$\nu_4(h)$
W	5	12361.2	265.1	
W	--	12368.1	272.0	
W	--	12370.5	274.4	hb of ν_4
S	2	12375.5	279.4	ν_4
M	1	12379.0	282.9	
W	0.5	12381.4	285.3	
W	0.5	12382.4	286.3	ν_5
W	1	12385.5	289.4	
W	10	12410.9	314.8	$\nu_5(h)$
W	10	12415.7	319.6	$\nu_5(h)$

Table 3. (continued...)

Intensity[a]	FWHM (cm^{-1})[b]	Vacuum Wavenumbers (cm^{-1})	$\Delta\nu$(origin) (cm^{-1})	Assignment
W	7	12596.7	500.6	$\nu_6 + \nu_5$
W	7	12601.0	504.9	
W	2	12662.3	566.2	$\nu_4 + \nu_5$
W	2	12665.9	569.8	
W	2	12668.2	572.1	
W	10	12740.9	644.8	$\nu_2(h)$
W	10	12749.9	653.8	
--	--	12771.2	675.1	hb of ν_1
--	--	12774.3	678.2	Pairs
--	--	12775.1	679.0	
--	--	12775.6	679.5	
M	0.5	12776.4	680.3	ν_1
--	1	12783.1	687.0	hb of ν_3
S	3	12787.8	691.7	ν_3; $\nu_3(h)$
W	--	12804.7	708.6	
W	1	12809.1	713.0	ν_2
W	1	12813.8	717.7	
W	--	12835.9	739.8	2 particle states
W	1	12837.2	741.1	$\nu_1(h)$
M	--	12861.5	765.4	$3\nu_4(h)$
W	--	12991.6	895.5	$\nu_1 + \nu_6$
W	--	12993.7	897.6	
W	--	12995.9	899.8	
W	--	13024.1	928.0	$\nu_2 + \nu_6$
W	--	13025.9	929.8	
W	--	13027.9	931.8	
W	--	13051.1	955.0	hb of $(\nu_1 + \nu_4)$
W	--	13055.3	959.2	$\nu_1 + \nu_4$
W	--	13059.3	963.2	
M	--	13073.3	977.2	$\nu_3 + \nu_5$
M	--	13077.5	981.4	
W	--	13455.1	1359.0	$2\nu_1$
M	--	13465.3	1369.2	$\nu_1 + \nu_3$
M	--	13495.5	1399.4	$\nu_3 + \nu_2$
M	--	13499.1	1403.0	

a. S = strong; M = medium; W = weak.
b. FWHM = full width at half maximum.
c. hb = hot band.
d. h = host.

Table 4. Vibrational site splittings (in cm^{-1}) for Γ_{7g} band of IrF_6/MF_6. The first number is the total splitting; a second number is given where appropriate for a three component splitting pattern.

	ν_2	$\nu_3{}^a$	ν_4	ν_5	ν_6
IrF_6/UF_6	8.6	1.9	4.5, 1.4	4.0, 0.7	6.3, 2.4
IrF_6/WF_6	5.3	-	3.6	3.9, 0.7	4.3, 1.8
IrF_6/MoF_6	4.7	<2.5	3.5	4.1, 1.0	4.4, 2.1

a. Due to a resonance between ν_3 of IrF_6 and ν_3 of WF_6, a meaningful upper limit on the site splitting cannot be given. It is expected to be similar to IrF_6/MoF_6.

Table 5. Splitting of the highest and lowest 4-fold degenerate $\Gamma_8(t_{2g})^3$ states by low-symmetry crystal field.

	Γ_{8g} $(^4A_{2g})^a$	Γ_{8g} $(^2T_{2g})$
Neat IrF_6	--	$(35.0)^b$
IrF_6/UF_6	10.0	66.4
IrF_6/WF_6	5.7	46.3
IrF_6/MoF_6	5.2	42.1

a. Splitting in ground states is obtained from hot band data; the hot band is not observed in neat IrF_6, probably due to the broad excitonic nature of the low lying state and magnetic ordering effects.

b. Exciton and magnetic effects also contribute to the observed splitting.

Table 6. Average vibrational frequencies in several $(t_{2g})^3$ electronic states of IrF_6/MoF_6. See Table 4 for site splittings in Γ_{7g} state.

	ν_1	ν_2	ν_3	ν_4	ν_5	ν_6
$\Gamma_{8g}(^2T_{2g})$	682	(716)[a]	696	284	218	217
$\Gamma_{7g}(^2T_{2g})$	680	715	692	281	287	217
$\Gamma_{8g}(^4A_2)$	701	646	720	275	264	205

a. Tentative assignment; see text for discussion.

Table 7. Summary of $\Gamma_{8g}(^2T_{2g})$ absorption spectra of mixed crystals of IrF_6/MoF_6 at 1.8K. Frequency uncertainty is 0.1 cm^{-1} for sharp lines.

Intensity[a]	FWHM (cm^{-1})[b]	Vacuum Wavenumbers (cm^{-1})	$\Delta\nu$(origin) (cm^{-1})	Assignment
--	--	14878.1	-5.2	hb[c] of origin
--	--	14880.8	-2.5	pair
S	1	14883.3 (6717.09Å)	0.0	origin (a)
--	--	14887.5	4.2	
--	--	14889.8	6.5	pair
--	--	14891.6	8.3	pair
--	--	14900.1	16.8	
S	10	14922.1	38.8	enhanced phonon[d]
S	10	14925.4	42.1	origin (b)
W	--	14932.4	49.1	
W	--	14937.6	54.3	
W	--	14945.7	62.4	
W	--	14951.3	68.0	phonons
W	--	14959.3	76.0	
W	--	14964.0	80.7	
W	--	14981.4	98.1	
W	--	14992.9	109.6	
W	20	15024.6	141.3	$\nu_6(a,h)$[e]
W	--	15062.7	179.4	$\nu_6(b,h)_1$
W	--	15073.1	189.8	
W	--	15080.9	197.6	hb of $\nu_5(a)$
M	2	15086.0	202.7	$\nu_5^1(a)$
M	2	15092.2	208.9	$\nu_5^2(a)$
S	7	15099.1	215.8	$\nu_6(a)$
S	--	15101.5	218.2	
W	--	15119.0	235.7	hb of $\nu_5^3(a)$
M	2	15124.8	241.5	$\nu_5^3(a)$
M	1	15128.8	245.5	$\nu_5^1(b)$
--	14	15135.1	251.8	$\nu_5^2(c)$
S	14	15137.7	254.4	$\nu_6(b), \nu_4(a,h)$
M	--	15155.1	271.8	$\nu_4(a,h), 2\nu_6(a,h)$
M	18	15162.6	279.3	$\nu_4^1(a), 2\nu_6(a,h)$
M	18	15168.0	284.7	$\nu_4^2(a), \nu_5^3(b), 2\nu_6(a,h)$
M	18	15176.2	292.9	$\nu_4(b,h)$
M	21	15201.9	318.6	$\nu_5(a,h)$
M	21	15212.4	329.1	$\nu_4(b)$

Continued...

Table 7. (continued)

Intensity[a]	FWHM (cm^{-1})[b]	Vacuum Wavenumbers (cm^{-1})	$\Delta\nu$(origin) (cm^{-1})	Assignment
W	3	15231.9	348.6	$\nu_5(b,h)$[f]
W	--	15244.3	361.0	$\nu_5(b,h)$
W	--	15299.9	416.6	
W	--	15302.4	419.1	$2\nu_5$ components[g]
W	--	15335.6	452.3	
W	--	15344.7	461.4	
W	15	15366.9	483.6	$\{\nu_4 + \nu_5^1\}(a)$
W	15	15371.1	487.8	$\{\nu_4 + \nu_5^2\}(a)$
W	15	15378.2	494.9	$\{\nu_4 + \nu_6\}(a)$
W	28	15405.0	521.7	$\{\nu_4 + \nu_5^3\}(a)$
W	28	15411.4	528.1	$\{\nu_4 + \nu_5^1\}(b)$
W	28	15416.2	532.9	$\{\nu_4 + \nu_5^2\}(b)$
W	28	15421.4	538.1	$\{\nu_4 + \nu_6\}(b)$
W	15	15437.6	554.3	
W	15	15444.8	561.5	$\{\nu_4 + \nu_5^3\}(b)$, $2\nu_4(a)$
W	16	15495.5	612.2	$2\nu_4$ (b)
W	--	15509.9	626.6	
W	--	15529.2	645.9	ν_2 (a,h)
W	--	15548.8	665.5	
W	1	15565.4	682.1	ν_1 (a)
W	--	15570.3	687.0	
W	--	15573.7	690.4	hb of ν_3 (a)
W	--	15577.4	694.1	ν_3 (a,h)
S	15	15579.6	696.3	ν_3 (a), ν_3 (a,h)
M	--	15604.3	721.0	ν_3 (a,h)
M	--	15607.5	724.2	ν_3 (a,h)
S	--	15618.2	734.9	ν_3 (b); ν_3 (b,h)
W	--	15625.8	742.5	ν_1 (a,h)
S	--	15648.1	764.8	$3\nu_4$ (a,h)
S	--	15687.4	804.1	
S	--	15689.8	806.5	$3\nu_4$ (b,h)
M	--	15715.0	831.7	
M	--	15728.8	845.5	
W	--	15755.6	872.3	
W	1	15767.3	884.0	$\{\nu_1 + \nu_5^1\}(a)$
W	2	15773.6	890.3	$\{\nu_1 + \nu_5^2\}(a)$
W	1	15781.1	897.8	$\{\nu_1 + \nu_6\}(a)$
W	1	15806.5	923.2	$\{\nu_1 + \nu_5^3\}(a)$
W	--	15810.4	927.1	$\{\nu_1 + \nu_5^1\}(b)$

Continued...

Table 7. (continued)

Intensity[a]	FWHM (cm^{-1})[b]	Vacuum Wavenumbers (cm^{-1})	$\Delta\nu$(origin) (cm^{-1})	Assignment
W	1	15816.5	933.2	$\{\nu_1 + \nu_5^2\}$(b)
W	1	15823.8	940.5	$\{\nu_1 + \nu_6\}$(b)
W	3	15847.7	964.4	$\{\nu_1 + \nu_4\}$(a)
W	3	15848.9	965.6	$\{\nu_1 + \nu_5^3\}$(b)
W	2	15858.7	975.4	$\{\nu_3 + \nu_4\}$(a)
W	--	15875.2	991.9	
M	--	15884.5	1001.2	$\{\nu_1 + \nu_4\}$(a)
M	--	15893.9	1010.6	$\{\nu_3 + \nu_4\}$(b)
S	--	15907.3	1024.0	Γ_{6g} or Γ_{7g} charge transfer state
M	--	15924.5	1041.2	
M	--	15934.9	1051.6	
M	--	15964.7	1081.4	one-phonon
M	--	15990.5	1107.2	
M	--	15995.1	1111.8	
W	--	16002.5	1119.2	
W	--	16030.5	1147.2	two-phonon
W	--	16042.3	1159.0	
W	--	16065.5	1182.2	
W	--	16077.1	1193.8	
W	--	16092.6	1209.3	
W	--	16119.4	1236.1	
W	--	16137.1	1253.8	
W	--	16182.8	1299.5	
W	--	16217.7	1334.4	
W	--	16226.6	1343.3	
W	--	16231.4	1348.1	
W	--	16246.2	1362.9	
W	--	16250.9	1367.6	
W	3	16259.4	1376.1	$\{\nu_1 + \nu_3\}$(a)
W	--	16296.2	1412.9	$\{\nu_1 + \nu_3\}$+ phonon (a)
W	--	16299.4	1416.1	$\{\nu_1 + \nu_3\}$(b)
W	--	16357.3	1474.0	
W	--	16370.7	1487.4	
M	--	16418.2	1534.9	
S	--	16449.6	1566.3	
S	--	16461.0	1577.7	
S	--	16469.0	1585.7	
S	--	16476.4	1593.1	
S	--	16485.1	1601.8	1024.0 + ν_1, ν_2, ν_3, phonons
M	--	16520.1	1636.8	
M	--	16545.2	1661.9	
M	--	16586.4	1703.1	
W	--	16616.9	1733.6	

Table 7. (continued)

Intensity[a]	FWHM (cm^{-1})[b]	Vacuum Wavenumbers (cm^{-1})	$\Delta\nu$(origin) (cm^{-1})	Assignment
W	--	17062.1	2178.8	
M	--	17086.8	2203.5	
M	--	17091.6	2208.3	$1024.0 + 2(\nu_1,$
W	--	17112.2	2228.9	$\nu_2, \nu_3)$
W	--	17124.8	2241.5	
W	--	17162.2	2278.9	

a. S = strong; M = medium; W = weak.
b. FWHM = full width at half maximum.
c. hb = hot band.
d. See text.
e. h = host.
f. Although this peak falls about 10 cm^{-1} outside the ν_5(b,h) exciton band, as approximated by the spread of $\underline{k}$ = 0 components, its line width and comparative behavior in MoF_6 and $\overline{W}F_6$ hosts indicates that it is a two-particle peak.
g. Lack of more data on ν_5 and ν_2 precludes parametric-type calculations which might identify these peaks specifically.

Figure 1.   Correlation diagram appropriate for the normal modes of an octahedral MF_6 molecule reduced to D_{4h} or C_s (σ_d) symmetry.

NORMAL MODE IN O_h D_{4h} C_s

ν_1 A_{1g} A_{1g}

ν_2 E_g B_{1g} A'

ν_5 T_{2g} B_{2g}

                                 E_g

ν_3, ν_4 T_{1u} A_{2u}

                                 E_u A''

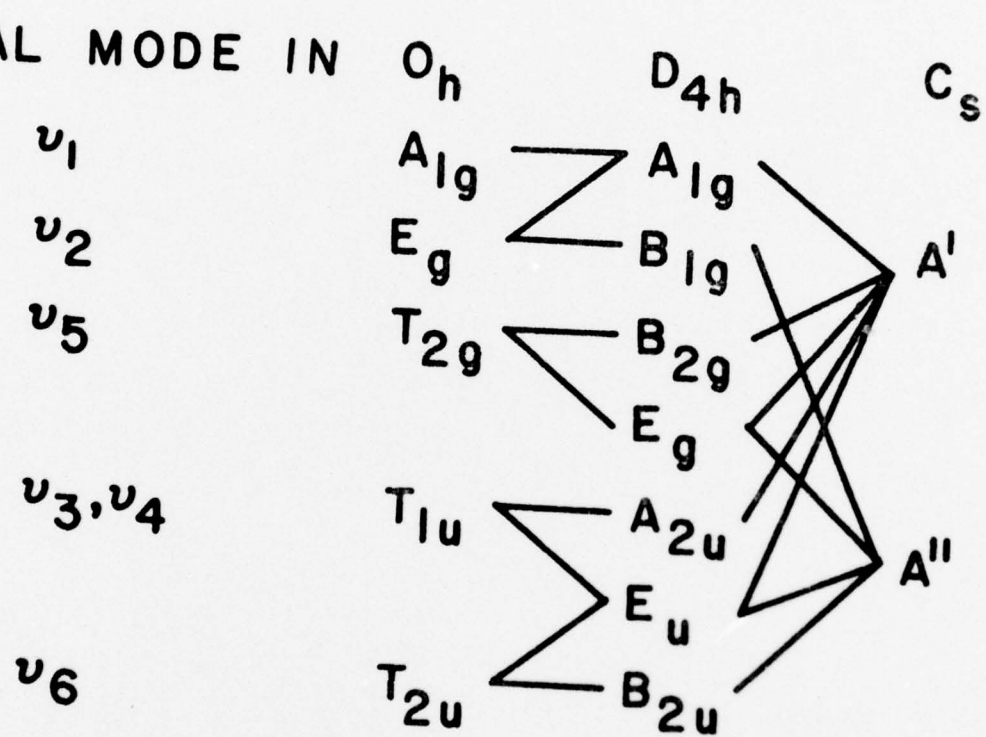ν_6 T_{2u} B_{2u}

Figure 2.   Energy levels of IrF_6. Rigorous symmetry labels (O_h^*) for

each electronic state are given, along with the cubic

Russell-Saunders state which correlates with the state for

vanishing spin-orbit coupling. Since all the final states are

gerade, the g label has been omitted in the right-hand column.
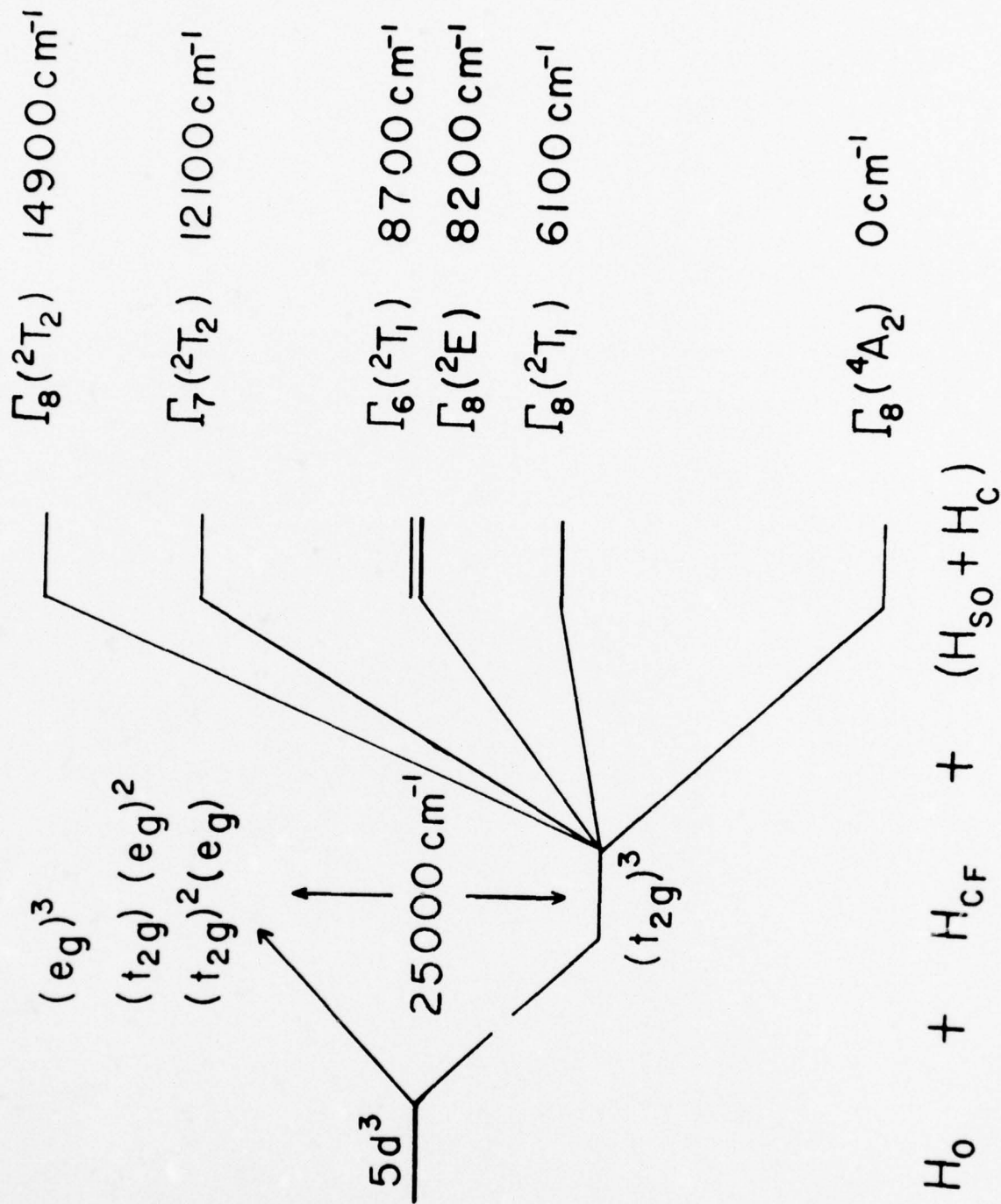
Energy Level Diagram
of IrF_6

$(e_g)^3$
$(t_{2g})(e_g)^2$
$(t_{2g})^2(e_g)$

$\Gamma_8(^2T_2)$ 14900 cm^{-1}

$\Gamma_7(^2T_2)$ 12100 cm^{-1}

$\Gamma_6(^2T_1)$ 8700 cm^{-1}

$\Gamma_8(^2E)$ 8200 cm^{-1}

$\Gamma_8(^2T_1)$ 6100 cm^{-1}

$\Gamma_8(^4A_2)$ 0 cm^{-1}

25000 cm^{-1}

$5d^3$

$(t_{2g})^3$

H_0 + H_{CF} + $(H_{SO} + H_C)$

Figure 3a.   Low resolution absorption spectrum of fundamental region of the $\Gamma_{7g}(^2T_{2g}) \leftarrow \Gamma_{8g}(^4A_2)$ transition for IrF_6/MoF_6.

Figure 3b.   Low resolution absorption spectrum of the $\Gamma_{8g}(^2T_{2g}) \leftarrow \Gamma_{8g}(^4A_2)$ transition of IrF_6/MoF_6.   Note the splitting of the origin and all the vibronic peaks.   Note, also, the unsplit origin of the even charge transfer (c.t.) state (see text).
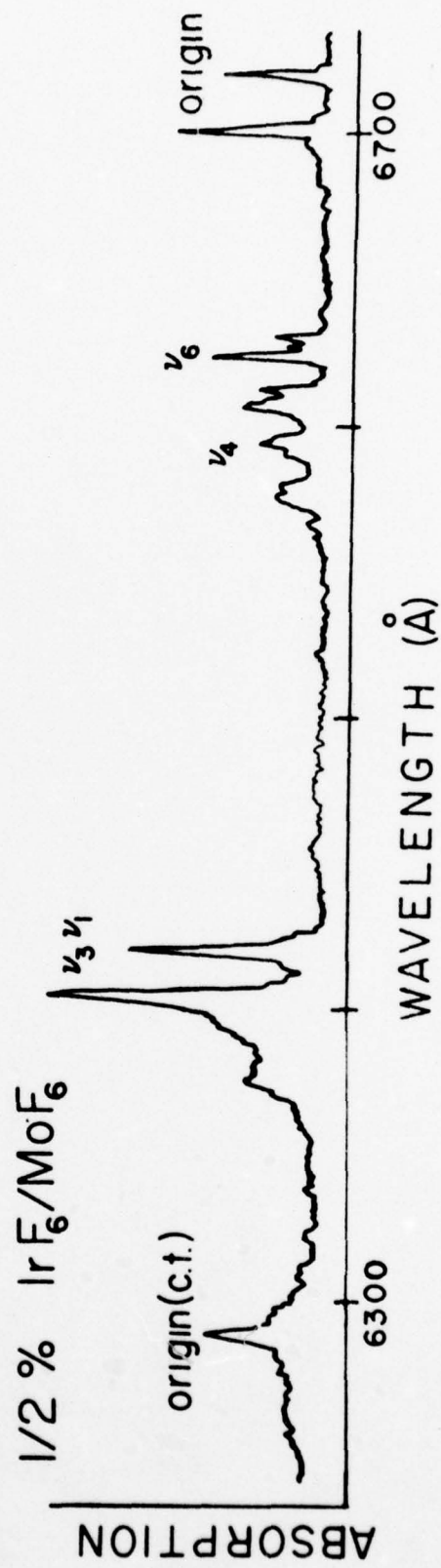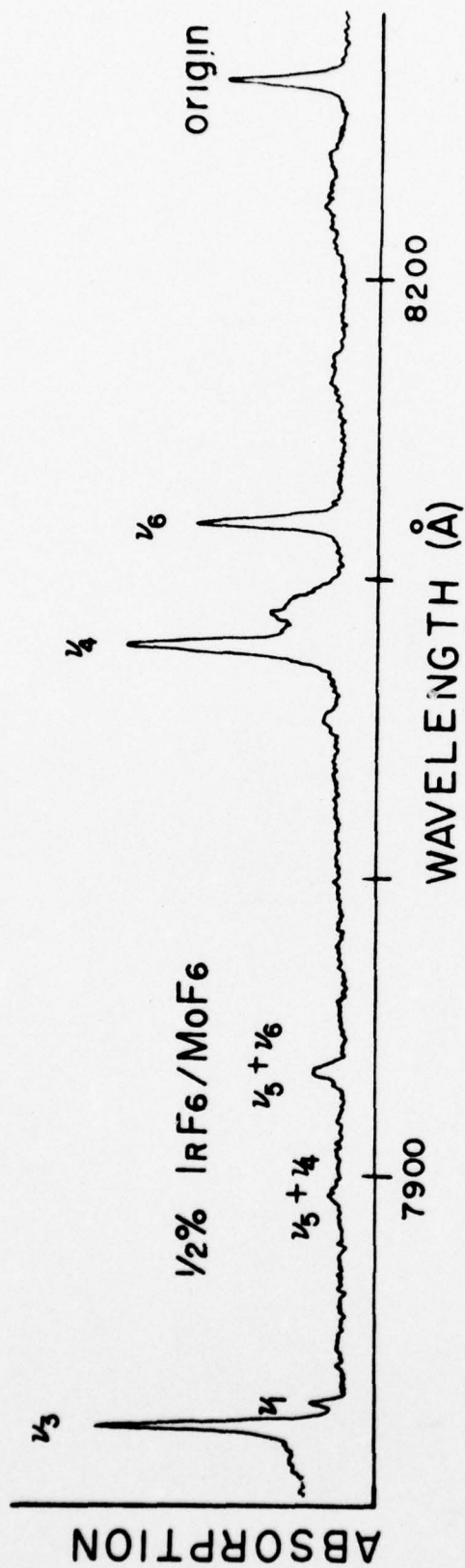
Top panel: ½% IrF₆/MoF₆

ν_3, ν_4, $\nu_5 + \nu_4$, $\nu_5 + \nu_6$, ν_4, ν_6, origin

Bottom panel: 1/2 % IrF₆/MoF₆

origin(c.t.), $\nu_3\nu_1$, ν_4, ν_6, origin

Axes: ABSORPTION (vertical), WAVELENGTH (Å) (horizontal)

Top scale: 7900, 8200

Bottom scale: 6300, 6700

Figure 4. ν_4, ν_5, ν_6 bending region of Γ_{7g} state of IrF_6/WF_6 at
            4.2K and 1.8K.   "hb" and "h" denote hot band and host,
            respectively.
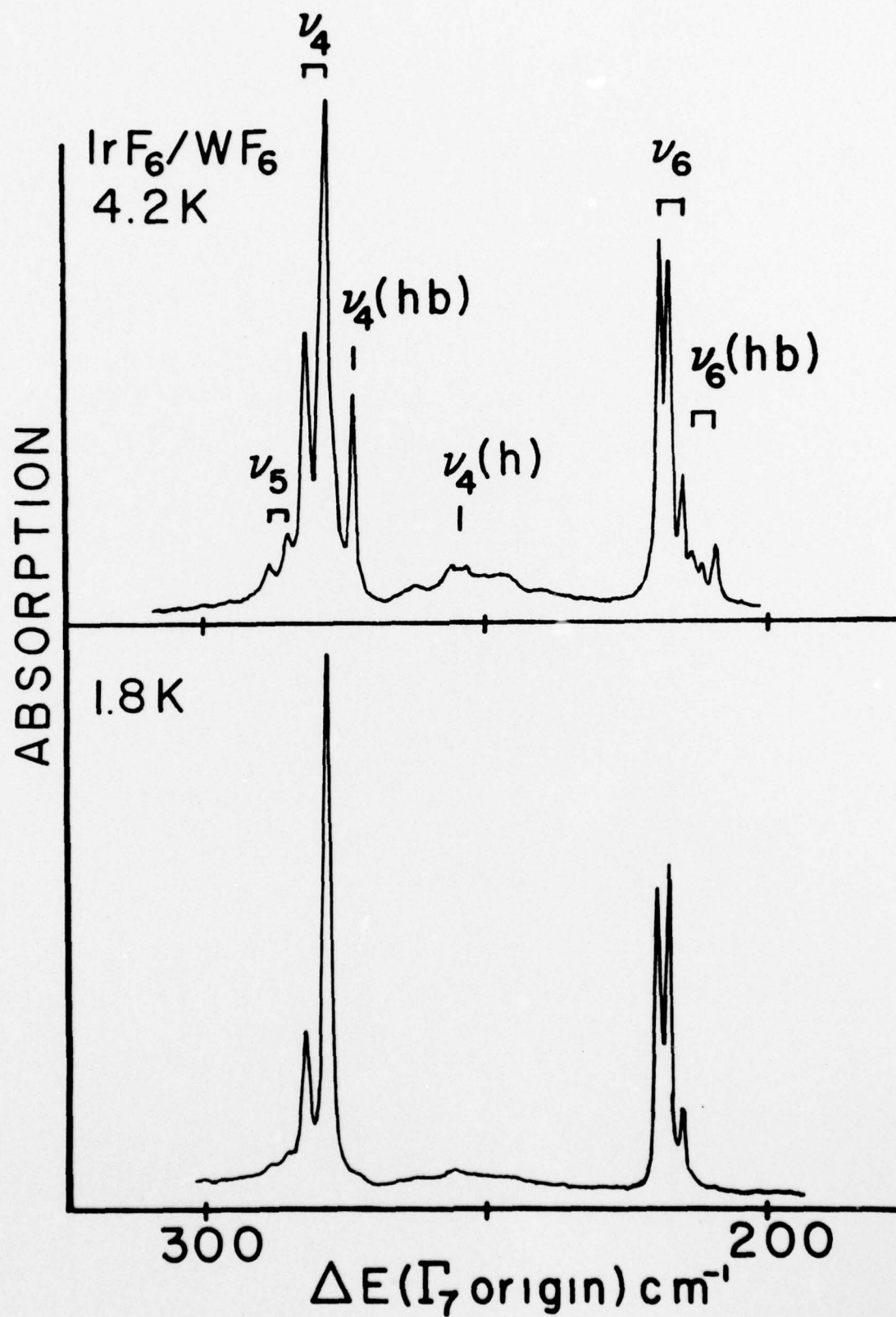
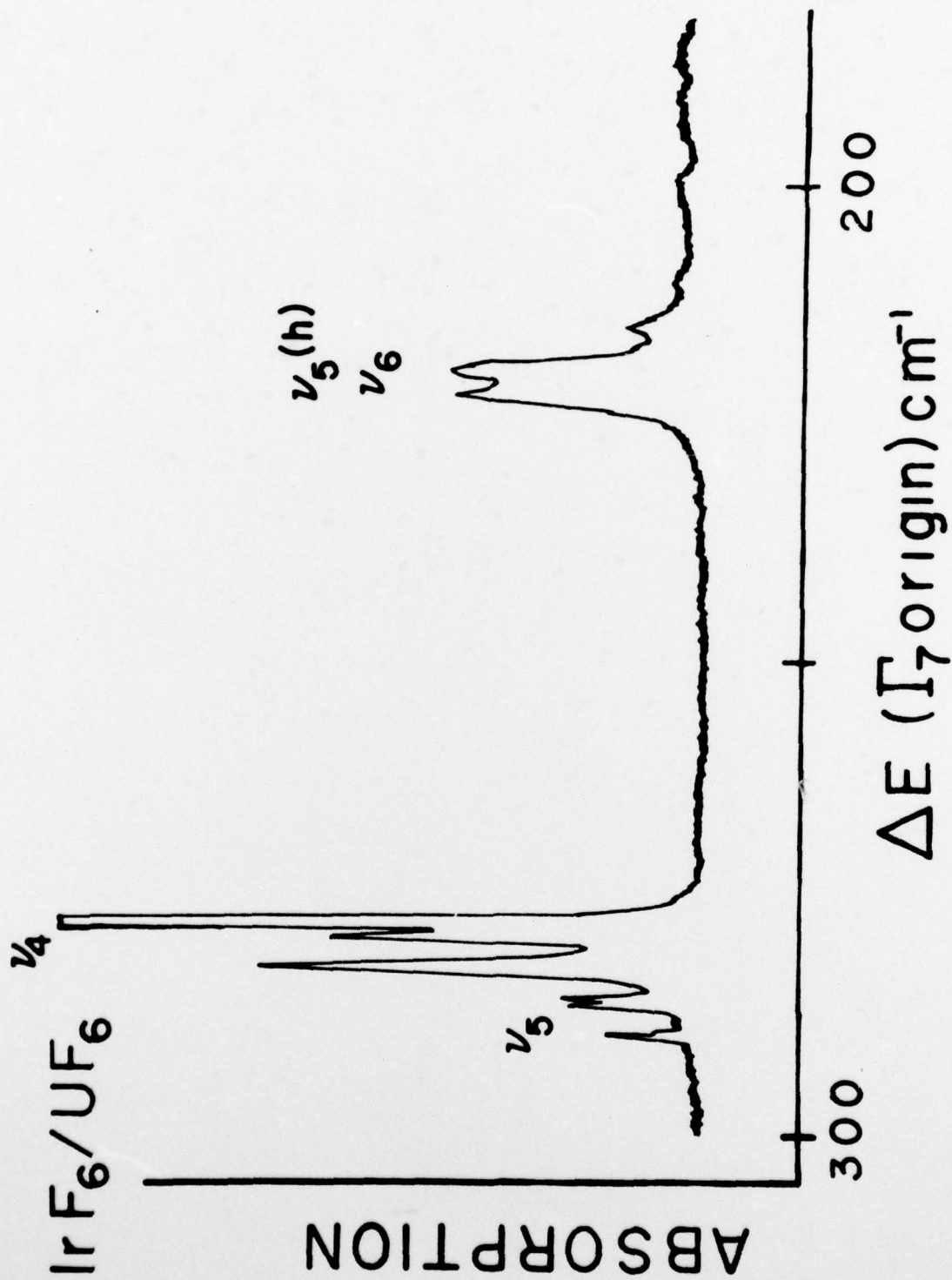Figure 5.   Bending region of Γ_7 state of IrF_6/UF_6 at 1.6K.

IrF_6/UF_6

ν_4

ν_5

$\nu_5(h)$

ν_6

ABSORPTION

$\Delta E\ (\Gamma_7\ \text{origin})\ cm^{-1}$

300

200

Figure 6.   Stretching region of Γ_7 state of IrF_6/MoF_6.

IrF_6 / MoF_6

$3\nu_4(h)$ $\nu_1(h)$ ν_2 ν_3 ν_1

ABSORPTION

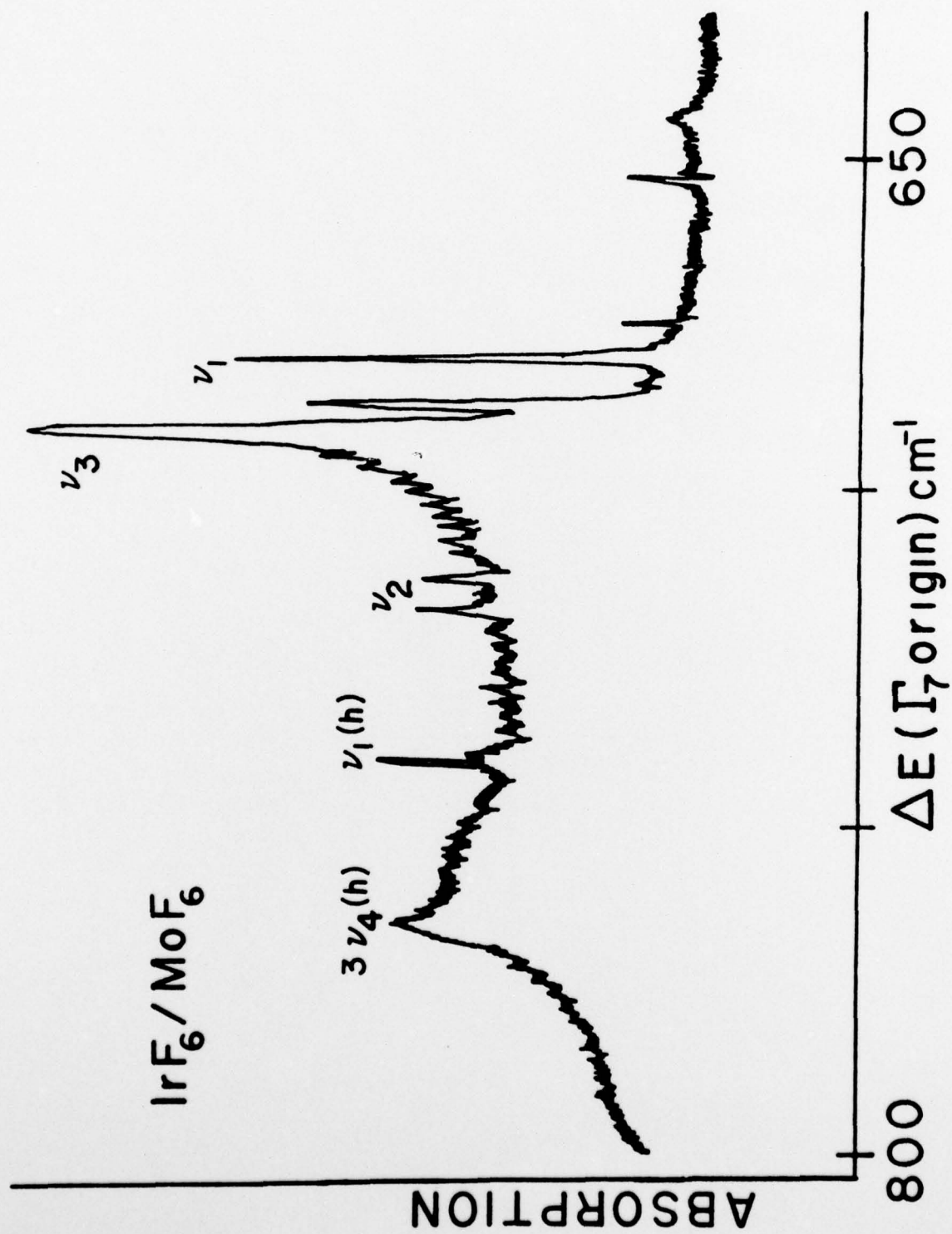$\Delta E\,(\Gamma_7\,\text{origin})\,\text{cm}^{-1}$

800   650

Figure 7.   Stretching region for Γ_7 state of IrF_6/UF_6 at 1.8K.
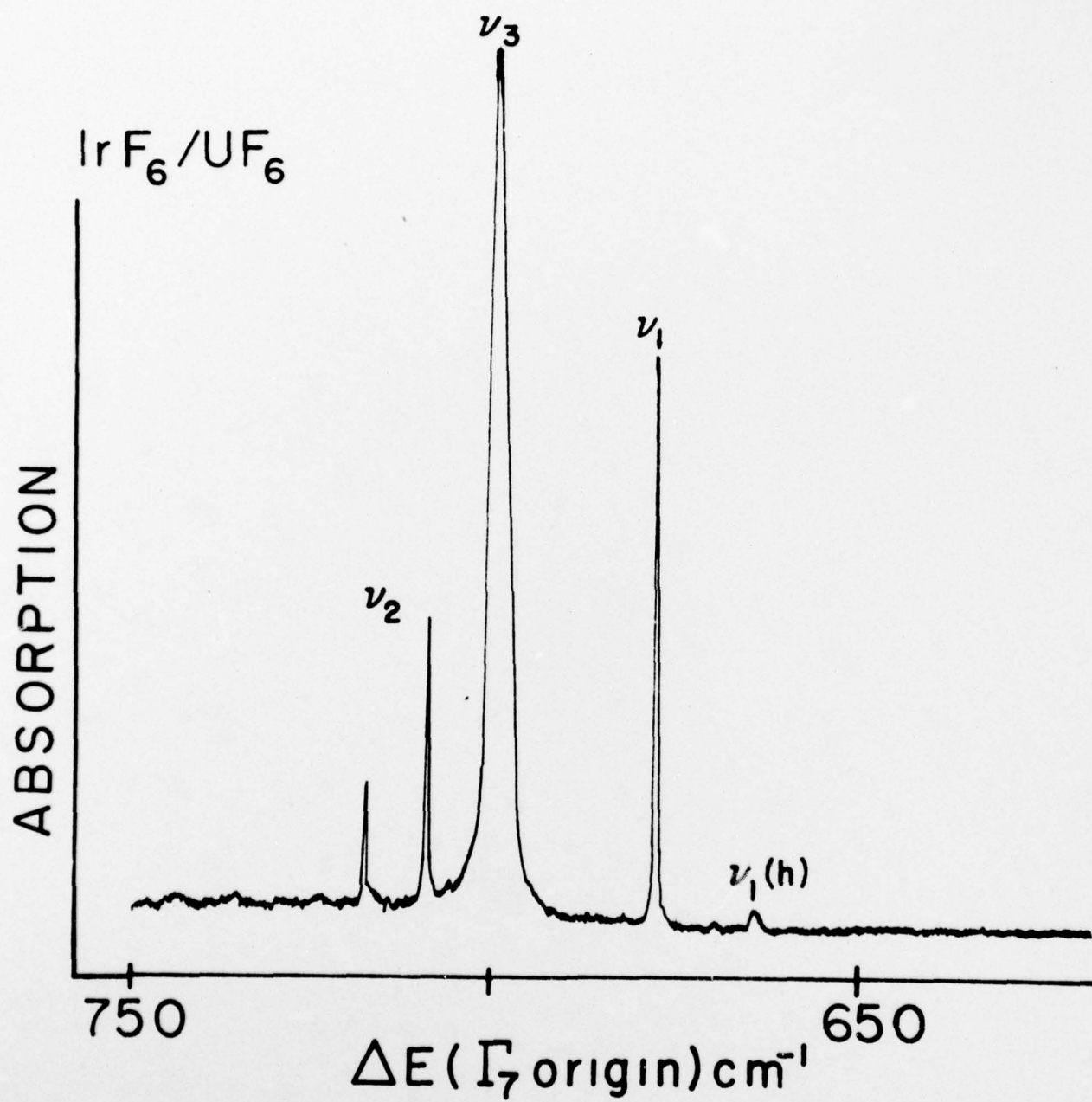
Figure 8.   Bending region of Γ_8 state of IrF_6/WF_6 at 1.8K.

IrF$_6$/WF$_6$

ν_5(b,h) ν_6(b,h) ν_4(b,h) ν_6(a,h) ν_5(a,h) ν_4(a,h)

ABSORPTION

ν_4(b) ν_5(b) ν_6(b) ν_4(a) ν_6(a) ν_5(a)

350 200

$\Delta E(\Gamma_8 \text{origin}) \text{cm}^{-1}$
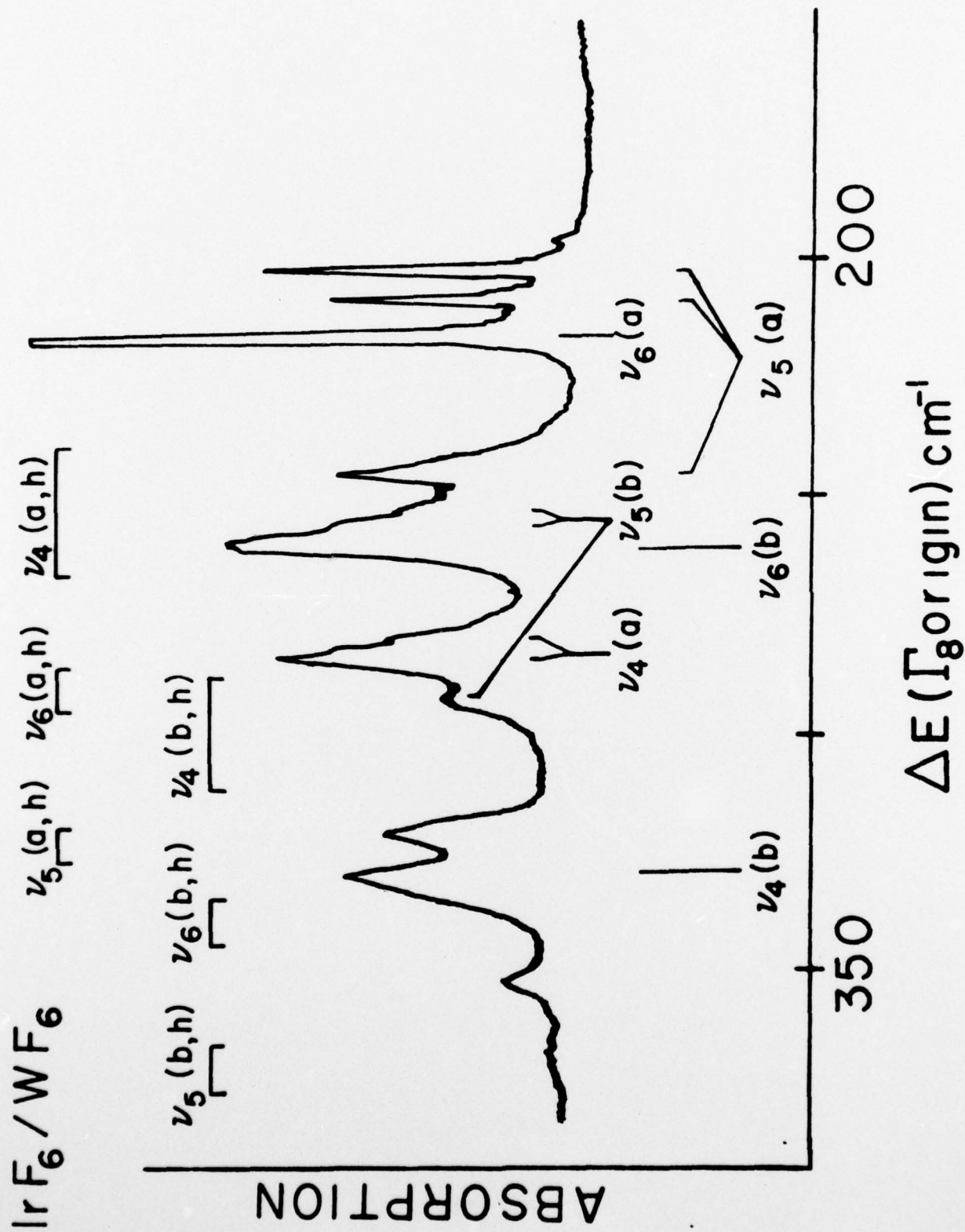
Figure 9.   Bending region of Γ_8 state of IrF_6/MoF_6 at 1.8K.

IrF$_6$/MoF$_6$

ν_5(a,h) ν_4(a,h)

ν_5(b,h)   2ν_6(a,h)

ν_4(b,h)

2ν_6(b,h)

ν_4(b)

ν_4(a)

ν_6(b)

ν_5(b)

γ

ν_6(a)

ν_5(a)

ABSORPTION

350   200

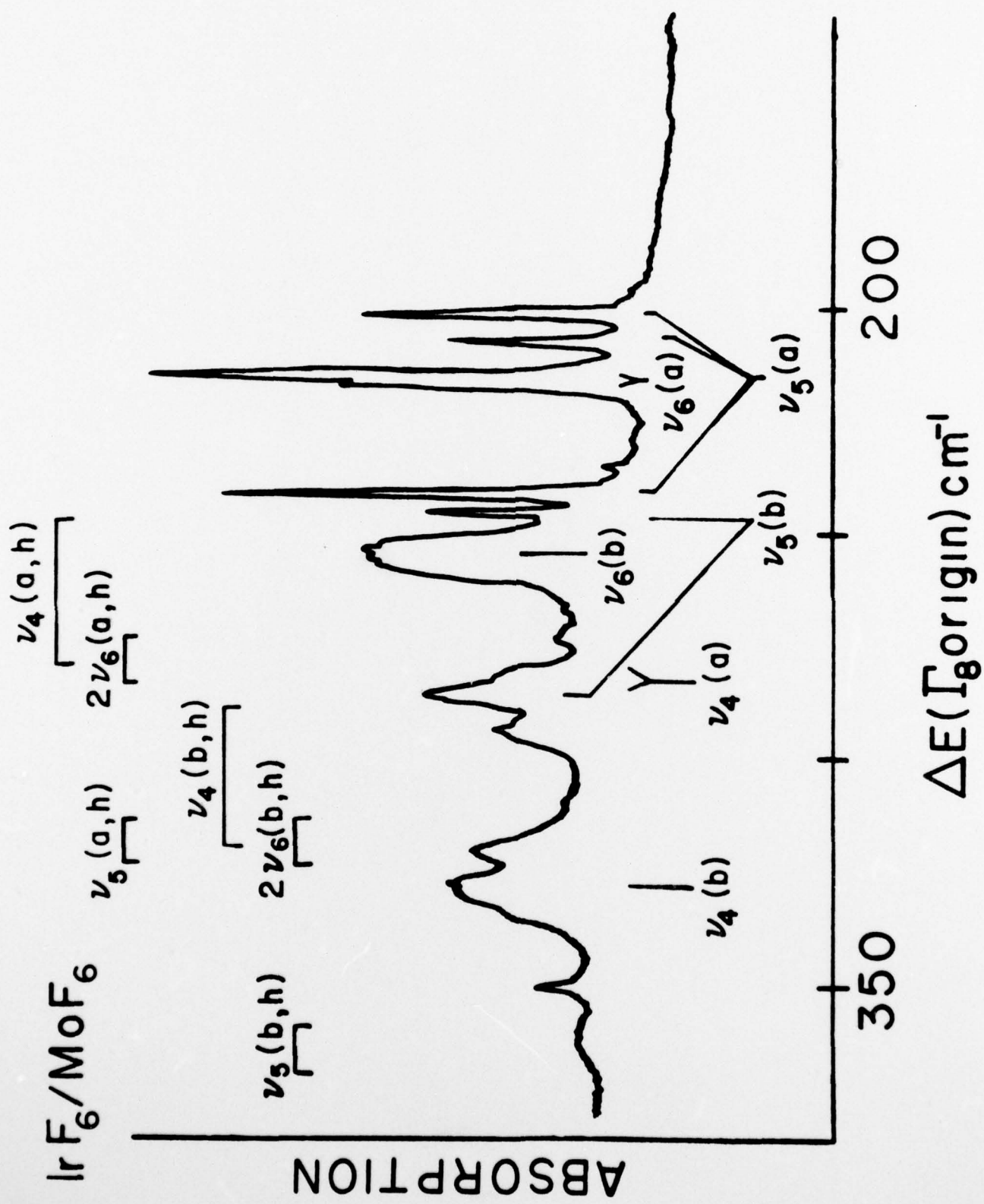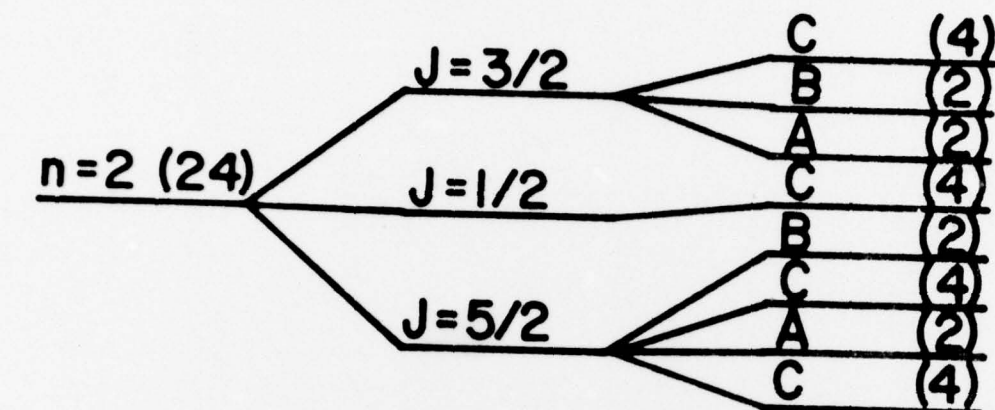$\Delta E(\Gamma_8 \text{origin}) \, cm^{-1}$

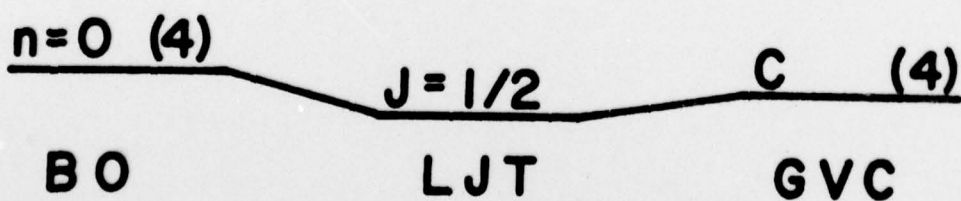Figure 10.   Schematic representation of lower vibronic energy levels for a
ν_5 (t_{2g}) vibration in a Γ_{8g} ($O_h^\star$) electronic state, in various
approximations: Born-Oppenheimer (BO), Linear Jahn-Teller
(LJT), and General Vibronic Coupling (GVC). Degeneracy of
some of the levels is given in parenthesis. Γ_i for GVC
levels refers to irreducible representations of $O_h^\star$.

C (4)

J=3/2

B (2)
A (2)

n=2 (24)

J=1/2

C (4)

B (2)
C (4)

J=5/2

A (2)

C (4)

A = Γ_6

B = Γ_7

C = Γ_8

J=1/2 C (4)

n=1 (12)

B (2)
A (2)

J=3/2

C (4)

n=0 (4)

J=1/2

C (4)
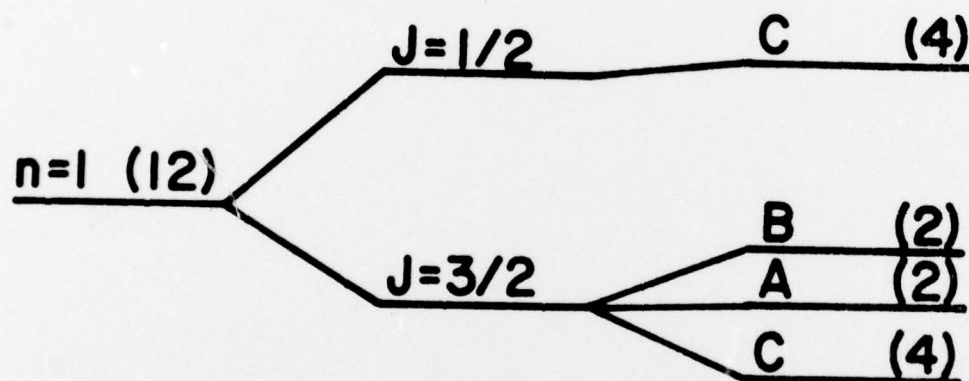
BO   LJT   GVC

TECHNICAL REPORT DISTRIBUTION LIST

No. Copies   No. Copie

	No. Copies		No. Copie
Office of Naval Research Arlington, Virginia 22217 Attn: Code 472	2	Defense Documentation Center Building 5, Cameron Station Alexandria, Virginia 22314	12
Office of Naval Research Arlington, Virginia 22217 Attn: Code 102IP	6	U.S. Army Research Office P.O. Box 12211 Research Triangle Park, North Carolina 27709 Attn: CRD-AA-IP	
ONR Branch Office 536 S. Clark Street Chicago, Illinois 60605 Attn: Dr. George Sandoz	1	Commander Naval Undersea Research & Development Center San Diego, California 92132 Attn: Technical Library, Code 133	1
ONR Branch Office 715 Broadway New York, New York 10003 Attn: Scientific Dept.	1	Naval Weapons Center China Lake, California 93555 Attn: Head, Chemistry Division	1
ONR Branch Office 1030 East Green Street Pasadena, California 91106 Attn: Dr. R. J. Marcus	1	Naval Civil Engineering Laboratory Port Hueneme, California 93041 Attn: Mr. W. S. Haynes	1
ONR Branch Office 760 Market Street, Rm. 447 San Francisco, California 94102 Attn: Dr. P. A. Miller	1	Professor O. Heinz Department of Physics & Chemistry Naval Postgraduate School Monterey, California 93940	
ONR Branch Office 495 Summer Street Boston, Massachusetts 02210 Attn: Dr. L. H. Peebles	1	Dr. A. L. Slafkosky Scientific Advisor Commandant of the Marine Corps (Code RD-1) Washington, D.C. 20380	1

Director, Naval Research Laboratory
Washington, D.C. 20390
Attn: Library, Code 2029 (ONRL)
     Technical Info. Div.
     Code 6100, 6170
	6
	1
	1		

The Asst. Secretary of the Navy (R&D) Department of the Navy Room 4E736, Pentagon Washington, D.C. 20350	1		
Commander, Naval Air Systems Command Department of the Navy Washington, D.C. 20360 Attn: Code 310C (H. Rosenwasser)	1		

TECHNICAL REPORT DISTRIBUTION LIST

No. Copies   No. Copies

Dr. M. A. El-Sayed   Dr. J. R. MacDonald
University of California   Code 6110
Department of Chemistry   Chemistry Division
Los Angeles, California 90024   1   Naval Research Laboratory
                                             Washington, D.C. 20375   1
Dr. M. W. Windsor
Washington State University   Dr. G. B. Schuster
Department of Chemistry   Chemistry Department
Pullman, Washington 99163   University of Illinois
                                             Urbana, Illinois 61801   1
Dr. B. R. Bernstein
Colorado State University   Dr. E. M. Eyring
Department of Chemistry   University of Utah
Fort Collins, Colorado 80521   Department of Chemistry
                                             Salt Lake City, Utah   1
Dr. C. A. Heller
Naval Weapons Center   Dr. A. Adamson
Code 6059   University of Southern California
China Lake, California 93555   1   Department of Chemistry
                                             Los Angeles, California 90007   1
Dr. G. Jones, II
Boston University   Dr. M. S. Wrighton
Department of Chemistry   Massachusetts Institute of Technology
Boston, Massachusetts 02215   Department of Chemistry
                                             Cambridge, Massachusetts 02139 1
Dr. M. H. Chisholm
Chemistry Department
Princeton, New Jersey 08540   1